INVESTIGATION OF THE EFFECTS OF SUMO MODIFICATION ON TWO CRITICAL PROTEINS: A PATHOGENIC NEK1 MUTANT THAT DRIVES ALS PATHOGENESIS AND THE CRISPR-ASSOCIATED CAS9 PROTEIN

by

Tunahan Ergünay

B.S., Molecular Biology and Genetics, Gebze Technical University, 2019

Submitted to the Institute for Graduate Studies in
Science and Engineering in partial fulfillment of
the requirements for the degree of
Master of Science

Graduate Program in Molecular Biology and Genetics
Boğaziçi University

2022

ACKNOWLEDGEMENTS

To begin with, I would like to thank several people who had a positive effect on me, supported and guide me with their knowledges during my education. My thesis supervisor Dr. Umut Sahin did not only guide and assist me with his knowledges, but he also influenced and shaped my academic and working ethics by being himself an excellent example of a discipline and rigorous scientist.

Also, my colleague Özgecan Ayhan was always supportive and helpful during the demanding journey of experiments and troubleshooting.

Egemen Şahin was the first student who was under my supervision, and I would like to specially thank him for his devotion and significant contribution to the project.

It would be impossible not mentioning and thanking Davod Khalafkhany, İrem Denizli and Ulduz Afshar for their guidance, brainstorming and material supports.

Nevertheless, the physical distance between us, Buse Nur Ural and Hasan Akyol were always mentally by my side with the endless support and I am sincerely thankful for this.

Most importantly, Enise Hatipoğlu, was near to me in every struggles on this period. I am thankful her for everything.

Nothing would be possible without the countless and unconditional support of my family, who are always there for me in my life.

Lastly, this project was supported by the funds of TÜBİTAK (119N095).

ABSTRACT

INVESTIGATION OF THE EFFECTS OF SUMO MODIFICATION ON TWO CRITICAL PROTEINS: A PATHOGENIC NEK1 MUTANT THAT DRIVES ALS PATHOGENESIS AND THE CRISPR-ASSOCIATED CAS9 PROTEIN

Small Ubiquitin-like modifier (SUMO) is an essential eukaryotic post-translational modification. SUMO isoforms attach to specific lysine residues on target substrates to modify their function, activity, solubility and stability. Dysregulation of sumoylation is associated with various pathological conditions ranging from cancer to neurodegeneration.

In this study, we focused on a mutant form of NEK1 protein, called truncated NEK1 (or tNEK1), which was recently linked to the pathogenesis of Amyotrophic Lateral Sclerosis (ALS). Previous studies from our lab had established that tNEK1 was prone to aggregation and associated with PML nuclear bodies (NBs). Here, we showed that PML also facilitates tNEK1 sumoylation and ubiquitylation. Furthermore, pharmaceutical agents that induce PML NB biogenesis, such as interferon-α (IFN), promote tNEK1 hypersumoylation in a PML-dependent manner. These findings have important implications for the management of tNEK1-linked ALS in the clinic, as IFN may promote the hypersumoylation, degradation, and clearance of this toxic protein in vivo, in a PML-dependent manner. In addition, our lab has created a transgenic mice model that expressed tNEK1 to study the effect of this mutation in vivo. In this study, we have performed motor neuron function assays (specifically, footprint and walking assays). Our results indicate that tNEK1-expressing mice display a walking disorder, implying that tNEK1 expression in vivo may lead to ALS pathogenesis.

Finally, we have also conducted studies on the CRISPR-associated Cas9 protein that we have recently discovered to be a sumoylation target. We have identified the major SUMO conjugation site on this protein and showed that sumoylation impacted on both the stability and DNA-binding ability of this important protein.

ÖZET

SUMO MODİFİKASYONUNUN İKİ KRİTİK PROTEİN ÜZERİNDE ETKİLERİNİN İNCELENMESİ: ALS PATOJENEZİNE SEBEP OLAN PATOJENİK NEK1 MUTANTI VE CRISPR İLE İLİŞKİLİ CAS9 PROTEİNİ

Küçük ubiquitin benzeri düzenleyiciler (SUMO) önemli bir translasyon sonrası modifikasyondur. SUMO izoformları hedef substrattaki spesifik lizin rezidülerine bağlanıp fonksiyonlarını, aktivitelerini, çözünürlüklerini ve stabilitelerini düzenler. Sumolanmanın bozukluğu kanserden nörodejenerasyona kadar çeşitli patolojik kondisyonlarla ilişkilendirilmiştir.

Bu çalışmada Amiloid Lateral Skleroz (ALS) hastalığının patojenezi ile ilişkilendirilmiş NEK1'in mutant versiyonu (tNEK1) üzerinde odaklandık. Laboratuvarımızın önceki çalışmalarında tNEK1'in çökelti oluşturmaya meylettiği ve PML nükleer cisimcikler (NB) ile etkileştiği saptanmıştır. Burada PML'in tNEK1'i sumolanmasını ve übikutilasyonunu desteklediğini gösterdik. Ayrıca, interferon-α (IFN) gibi PML NB biyogenezini indükleyen ilaçlar ile tNEK1 hipersumolanmasının PML'e bağlı olarak sağladığını gösterdik. IFN bu toksik proteinin in vivo olarak PML ilişkili hipersumolanmasını, yıkımını ve arındırmasını destekleyebileceği için bu bulguların tNEK1'e bağlı ALS'nin yönetimi için önemli klinik çıktıları bulunabilir. Ek olarak, tNEK1'in organizmada etkilerini çalışmak için laboratuvarımızda bu mutantı eksprese eden transgenik fare modelleri oluşturuldu. Bu çalışmada motor nöron fonksiyon deneyleri (özellikle ayak izi ve yürüme) gerçekleştirdik. Sonuçlara göre tNEK1 eksprese eden farelerin in vivo ortamda ALS patogenezine yol açabileceğini ima eden bir yürüme bozukluğu sergilemektedirler.

Son olarak, CRISPR ilişkili Cas9 proteini üzerinde çalışmalar yürüttük ve yakın zamanda bu proteinin bir SUMO hedefi olduğunu keşfettik. Bu protein üzerinde SUMO konjügasyon bölgesini tanımladık ve sumolanmanın Cas9 stabilitesini ve DNA bağlanma yetisine etki ettiğini keşfettik.

TABLE OF CONTENTS

LIST OF FIGURES

LIST OF TABLES

LIST OF SYMBOLS

A	Amper
bp	Base pair
cm^2	Square centimeter
g	Gram
g	Gravity
h	Hour
kDa	Kilodalton
M	Molar
mg	Milligram
ml	Milliliter
mM	Millimolar
mm	Millimeter
ng	Nanogram
V	Volt
α	Alpha
β	Beta
μg	Microgram
μl	Microliter
μM	Micromolar
^{o}C	Degree Celsius

LIST OF ACRONYMS/ABBREVIATIONS

Aβ	Amyloid Beta
ALS	Amyotrophic Lateral Sclerosis
APL	Acute Promyelocytic Leukaemia
As	Arsenic
As-R/L	Asymmetry of forelimb and hindlimb (Right or left limb)
As_2O_3	Arsenic Trioxide
ATL	Adult T-cell lymphoma
ChIP	Chromatin Immunoprecipitation
CRISPR	Clustered Regularly Interspaced Palindromic Repeats
crRNA	CRISPR RNA
CTAB	Cetyltrimethylammonium bromide
dCas9	dead Cas9
DDR	DNA damage repair
DMEM	Dulbecco's Modified Eagle Medium
DUB	Deubiquitinase
eCas9	enhanced Cas9
fALS	familial ALS
FBS	Fetal bovine serum
FS-R/L	Forelimb stride length (Right or left limb)
gRNA	guide RNA
HBS	HEPES-buffered saline
HD	Huntigton’s disease
HDR	Homology-directed repair
HS-R/L	Hindlimb stride length (Right or left limb)
HTLV-1	Human T-cell Lymphotropic Virus Type-1
IF	Immunofluorescence
IFN	Interferon-α
IP	Immunoprecipitation
KI	Knock-in

KO	Knock-out
LB	Luria Bertani
LLPS	Liquid-liquid phase separation
MS	Mass Spectrometry
NB	Nuclear Body
nCas9	Cas9 nickase
NEK1	NIMA-related kinase 1
NEM	N-ethylmaleimide
NES	Nuclear Export Signal
NHEJ	Nonhomologous End Joining
NLS	Nuclear Localization signal
OFH-R/L	Overlap between forelimb and hindlimb (Right or left limb)
PBS	Phosphate-buffered saline
PD	Parkinson's disease
PIC	Protease inhibitor cocktail
PKD	Polycystic kidney disease
PLA	Proximity ligation assay
PTM	Posttranslational modification
RIPA	Radioimmunoprecipitation assay buffer
sALS	sporadic ALS
SDM	Site directed mutagenesis
SDUB	SUMO deubiquitinase
SEM	Standard error of the mean
SENP	Sentrin-specific protease
SIM	SUMO-interacting motif
siPML	small-interfering PML
siRNA	small-interfering RNA
SMD	spondylometaphyseal dysplasia
STUbL	SUMO-targeted Ubiquitin ligase
SUMO	Small Ubiquitin-like modifier
t/t	homozygous tNEK1
TALEN	transcription activator-like effector nuclease
TBS	Tris-buffered saline

tNEK1	truncated NEK1
tracrRNA	transactivating crRNA
UBL	Ubiquitin like protein
WF	Width of Front base
WH	Width of Hind base
wo	weeks old
ZFN	Zinc-finger nuclease

1. INTRODUCTION

1.1. Post-translational Modifications

Several factors and mechanisms lie beneath the complexity of biological systems. It is known that the number of genes is increased in more advanced and complex organisms. In addition to this, the post-translational modifications (PTMs) of proteins in eukaryotic systems contribute to a higher complexity. PTMs can change the properties of a protein through reversible or irreversible attachment to amino acid side chains on a protein. They can affect protein interactions, cellular localization, chromatin remodeling, functional activity, protein stability, global structure and its dynamics (Figure 1.1). More than 400 types of PTMs have been discovered, and 5% of the proteome plays a role in mediating PTMs. Among those PTMs, the most studied modifications are phosphorylation, acetylation, ubiquitylation, and methylation. They are ATP-dependent processes involved in many biological activities, such as cell metabolism, immunogenetics, cell cycle, and cell survival (Ramazi and Zahiri, 2021).

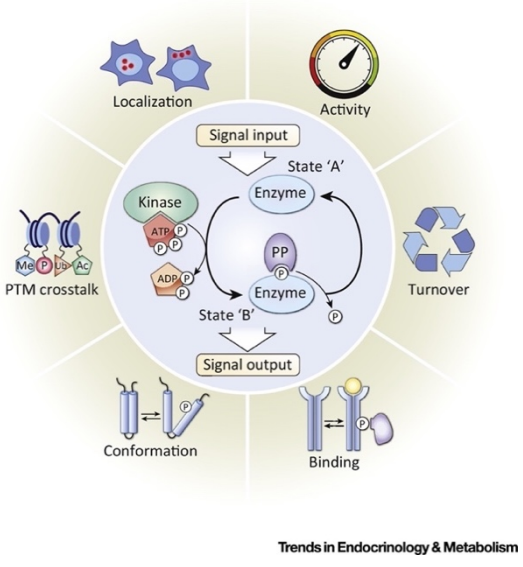

Figure 1.1. Effects of post-translational modifications. Phosphorylation of a protein is showed as an illustration. Reprinted from Trends in Endocrinology & Metabolism, Elsevier.

1.2. Ubiquitin and Ubiquitin-like Proteins

Ubiquitylation is one of the well-studied PTMs involved in almost all cellular processes (Swatek and Komander, 2016). Ubiquitin is a 76-amino acid protein that gets attached to the target protein's lysine (K) residues. Ubiquitylation is a reversible process and is generally involved in proteasomal degradation or endocytic trafficking of proteins. In addition, it is also related to protein translation and DNA repair (Miranda and Sorkin, 2007). The attachment of Ubiquitin to its target occurs in three distinct steps: (1) activation of Ubiquitin by cleavage of the C-terminus, which exposes diglycine residue (GG), and ATP-dependent attachment to the Ubiquitin-activating enzyme (E1), (2) transfer of Ubiquitin to Ubiquitin-conjugating enzyme (E2), and (3) attachment of Ubiquitin to the target protein's lysine residue by Ubiquitin ligase (E3) (Rape, 2018) (Figure 1.2). Ubiquitin can also be ubiquitylated on seven lysine residues on the peptide, which results in the formation of poly- or mono-Ubiquitin chains on the target protein (Swatek and Komander, 2016). Polyubiquitin chains on different lysine residues lead to different outcomes such as DNA damage response, and lysosomal degradation that's mostly linked with proteasomal degradation of the target protein. It should also be noted that detachment of Ubiquitin is facilitated by de-ubiquitinases (DUBs).

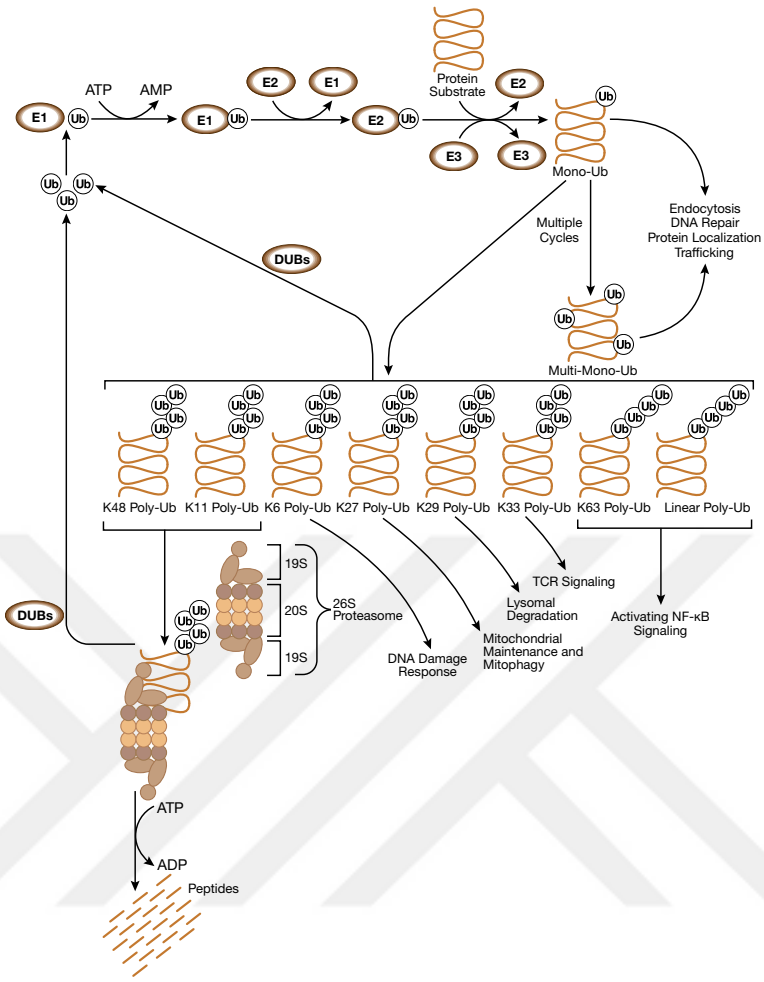

Figure 1.2. Ubiquitylation mechanism. Illustration reproduced courtesy of Cell Signaling Technology, Inc.

At the end of the 20th century, several protein families called ubiquitin-like proteins (UBLs) were discovered; they share evolutionary relations with Ubiquitin, such as their folding structure and the enzymes (E1, E2 and E3) that are involved. The UBL conjugation process is similar to ubiquitylation: (1) activation of the UBL protein and its recognition by a conjugating enzyme, (2) attachment to a target protein, and (3) formation of UBL chains and, optionally, interaction with other PTMs (Cappadocia and Lima, 2018). In the evolutionary process, UBLs are divided into two types: type-I UBLs, and type-II UBLs, with the former able to be conjugated but not the latter. On the one hand, type-II UBLs are rarely seen modifications that have E1-activating and E3-ligating enzymes and fold autonomously without the requirement for conjugation. On the other hand, type-I UBLs are more abundant and require conjugation. Families included in type-I UBLs are SUMO, NEDD8, ATG8, ATG12, URM1, UFM1, FAT10 and ISG15 (Figure 1.3) (Cappadocia and Lima, 2018).

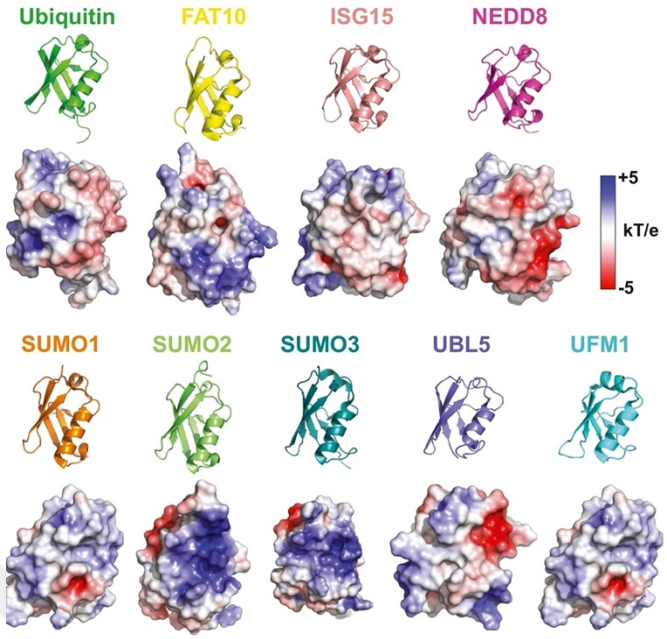

Figure 1.3. 3D structures of Ubiquitin and Ubiquitin-like proteins (Vaughan *et al*., 2021).

1.3. SUMO Modification

In 1995, a small protein called Smt3 was discovered in *Saccharomyces cerevisiae*, and this protein was included later in a protein family called Small Ubiquitin-like Modifier (SUMO) (Meluh and Koshland, 1995). SUMO is a small protein the size of 13kDa, which shares a common identity with the Ubiquitin protein. In humans, there are five functional SUMO isoforms enumerated from 1 to 5. Since SUMO2 and SUMO3 are similar and share 95% identity, they are generally called SUMO2/3. In addition, SUMO1 shares 45% of its sequence identity with other SUMO proteins. While SUMO1 and SUMO2/3 are ubiquitously expressed, the expression of SUMO4 and SUMO5 is restricted to specific tissues and organs, and they are expressed under stress conditions (Celen and Sahin, 2020; Vaughan *et al*., 2021).

As mentioned in the previous chapter, three enzymes like type-I UBLs are involved in sumoylation. These enzymes are E1 SUMO-activating enzyme (SAE1, SAE2), E2 SUMO-conjugating enzyme (UBC9), and E3 SUMO ligase (Figure 1.4). It should be noted that sumoylation can occur without the requirement for an E3 ligase that provides substrate

specificity. Besides, UBC9 is the only E2 enzyme that is essential for sumoylation. It was reported in the literature that UBC9 knock-out mouse models did not survive because of defects in embryonic develeopment. For sumoylation, a consensus motif "ψKxD/E" (where ψ stands for a hydrophobic residue, K stands for the lysine residue that SUMO peptides attach to, X stands for any amino acid, and D/E stands for aspartic acid and glutamic acid, respectively) is required on the surface of a protein. After the recognition of the motif, activated SUMO is covalently attached to the lysine residue with the help of a conjugating enzyme, UBC9. Since SUMO protein also contains that motif itself, mono and poly SUMO chains form like Ubiquitin. For example, K11 residue on SUMO2/3 is topologically more favourable for making poly-SUMO chains. In addition, SUMO can also be modified by other PTMs, such as ubiquitylation, acetylation, and phosphorylation (Celen and Sahin, 2020).

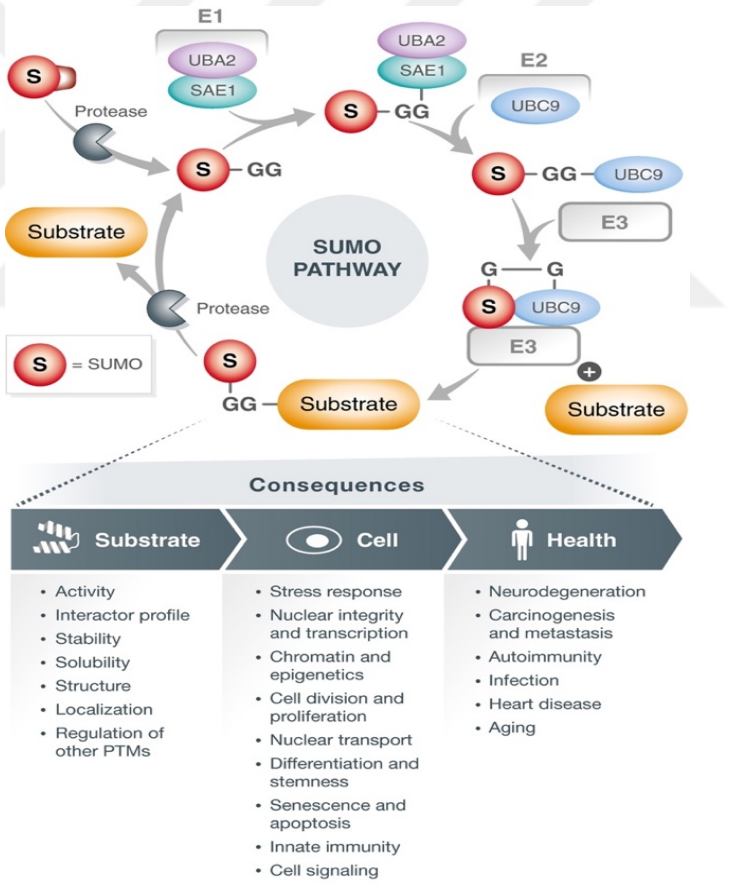

Figure 1.4. Sumoylation pathway and its consequences in substrate, cellular and organism's health level (Celen and Sahin, 2020).

As a feature of UBLs, sumoylation is also a reversible process; the responsible enzymes for desumoylation are called Sentrin-specific proteases (SENPs). In humans, the

family contains six members, and they recognize different SUMO paralogs that cause the deconjugation of SUMO. In addition, SENPs also play a role in the maturation of SUMO by cleaving the C-terminus to expose GG residue (Chang and Yeh, 2020).

Sumoylation plays a vital role in many processes such as protein stability, chromatin remodelling, subcellular localization, protein-protein interaction, and intracellular signalling. For instance, sumoylation can alter protein stability by enhancing or inhibiting ubiquitylation (Celen and Sahin, 2020; Liebelt and Vertegaal, 2016). There are proteins called SUMO-targeted Ubiquitin ligase (STUbL) and SUMO deubiquitinase (SDUB) that function as an addition or removal of Ubiquitin to or from the SUMO, which affects protein stability (Liebelt and Vertegaal, 2016). Another essential role of SUMO is to make noncovalent interactions between a sumoylated protein and a target protein containing hydrophobic stretches called SUMO Interacting Motif (SIM). For example, SIMs located on SUMO promote interaction with a SUMO chain on a donor protein and cause Ubiquitin to be added to it or its conjugation to another lysine residue that subsequently leads to degradation of the target protein (Celen and Sahin, 2020; Chang and Yeh, 2020).

Sumoylation also promotes the nuclear import or export of proteins. Sumoylated proteins that have nuclear localization signal (NLS) are imported to the nucleus by interacting with importin. The reverse reaction facilitates the export of proteins from the nucleus. Sumoylation has a dual role in the protein export from the nucleus by stimulating or inhibiting it (Ptak and Wozniak, 2017). Moreover, it is also known that proteins' recruitment to PML nuclear bodies in the nucleus is promoted by sumoylation (Sahin *et al*., 2014).

1.4. PML Nuclear Bodies

Promyelocytic leukemia nuclear body (PML NB) is a eukaryotic membraneless organelle inside the nucleus. The formation of PML NBs is based on the principle of liquid-liquid phase separation (LLPS), like nucleoli and P bodies. PML NBs mostly contain PML proteins, located in the shell, and some other proteins such as Sp100, Daxx and p53, located in the core. As a feature of membraneless organelles, PML NBs have some characteristic

features: phase separation (separation of distinct liquids like water and oil), fusion and fission (two nuclear bodies can fuse and divide) and reformation (if the compartment is disrupted temporarily, it restores itself). PML protein is crucial for the forming PML NBs; in the absence of PML NBs, the other proteins supposed to be located inside of the PML NB would disperse in the nucleus (Lallemand-Breitenbach and de Thé, 2018; Peng *et al*., 2021; Sahin *et al*., 2014).

PML NBs are involved in several cellular processes such as stress response, senescence, and apoptosis. Biogenesis of these bodies can be induced by oxidative stress or drugs such as arsenic and interferon. PML NB biogenesis occurs by PML oxidation, UBC9 conjugation, and sumoylation of PML whose role is to act as a biological glue for the shell of the nuclear body (Figure 1.5). Recruitment of partner proteins lead to sumoylation and SUMO-SIM interaction in the core. Therefore, PML NBs provide a SUMO-enriched environment for sumoylated and SIM-containing proteins in the nucleus, which facilitates the clearance of misfolded, aggregated, and viral proteins, DNA damage response, regulation of self-renewal, and control of cellular metabolism (Sahin *et al*., 2014).

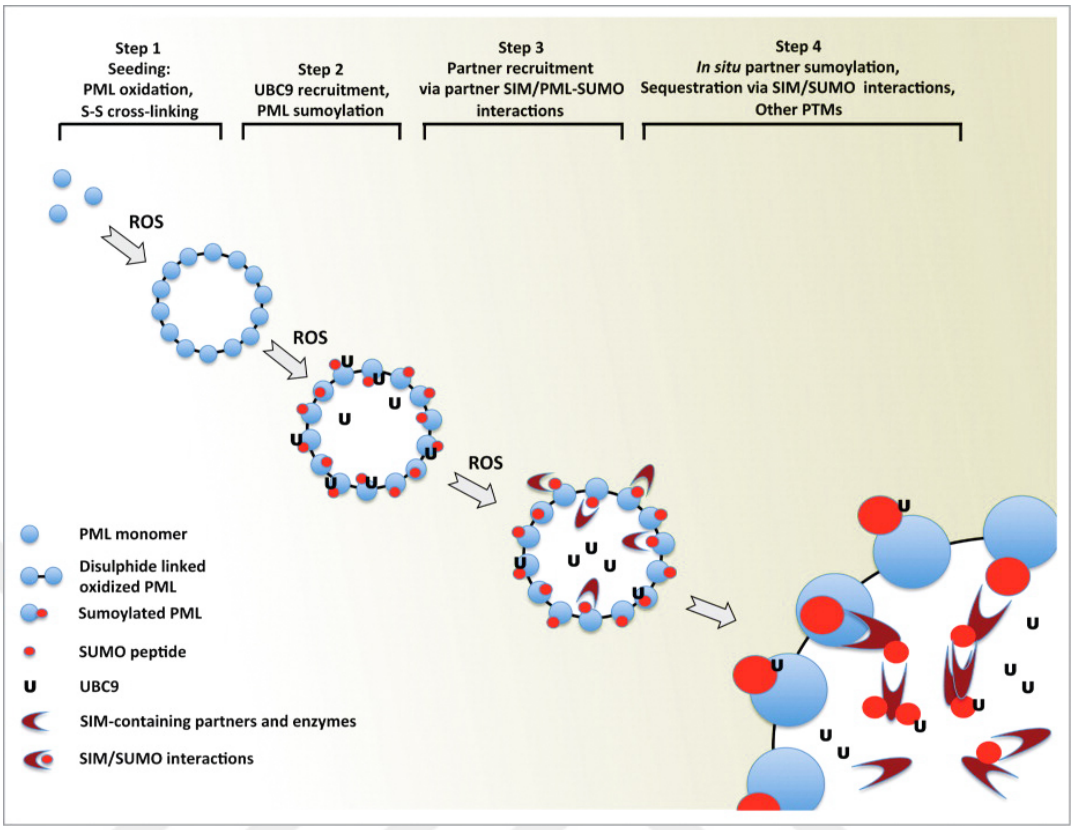

Figure 1.5. PML biogenesis. In the presence of Reactive Oxygen Species (ROS), PML oxidation and disulfide links occurs. This allows UBC9 recruitment which results in PML sumoylation. This primary stucture of PML body allows partner protein recruitment provided by SIM/PML-SUMO interactions. Finally, nuclear bodies allow protein sumoylation and other PTMs.

Since PML NBs play an essential role in cellular processes, several studies aim to treat some diseases by utilizing and taking advantage of the role of this prominent PML NB. A splendid example is arsenic, which is already being used as a therapeutic agent for Acute Promyelocytic Leukemia (APL) treatment. PML sumoylation is enhanced, which in turn promotes subsequent degradation of toxic proteins. Besides, the pathogenesis of neuro-degenerative diseases (i.e., Huntington's, ataxia) is suggested to correlate with the absence of PML NBs. It was also shown that interferon or arsenic treatment recruits SUMO peptides to Tax protein, causing hypersumoylation of this protein and subsequent proteasomal degradation (Sahin *et al.*, 2014).

1.5. SUMO in Neurodegeneration

SUMO plays a significant role in various diseases and conditions such as infection, cancer, neurodegeneration, heart failure, and atherosclerosis. SUMO modification can cause the aggregation of toxic proteins or the degradation of aggregated proteins related to neurodegeneration (Celen and Sahin, 2020). As an example, the Tau protein promotes Alzheimer's disease by forming neurofibrillary structures. SUMO modification of Tau increases the protein's stability, which may contribute to disease progression (Luo *et al*., 2014). Besides, the Parkinson's disease related protein α-synuclein was shown to be sumoylated. Sumoylation of this protein results in its increased solubility and prevention of the Lewy body formation (Shahpasandzadeh *et al*., 2014).

1.6. Amyotrophic Lateral Sclerosis

Amyotrophic lateral sclerosis (ALS) is a fatal neurodegenerative disease that primarily affects motor neurons of the spinal cord, brain, and brain stem. The principal clinical diagnosis of ALS is the dysfunction of the upper and lower motor neurons, which causes global muscle weakness, involuntary weight loss and respiratory dysfunction. Even though the disease mostly manifests in patients in adulthood, there were also some cases diagnosed in childhood (Siddique and Siddique, 2021; Kiernan *et al*., 2011).

ALS disease comes in two types according to its causal effect: familial ALS (fALS), and sporadic ALS (sALS). The former exhibits Mendelian pattern of inheritance while the latter is the result of a combination of genetic and environmental factors. While 90-95% of the cases belonging to sALS are caused mainly by chronic occupational exposure to lead, the remaining are transmitted in an autosomal dominant way (Figure 1.6a, b). More than 50 genes have been identified to be associated with ALS, with four of them, SOD1, C9orf72, FUS, and TARDP, being the most often found in ALS pathogenesis (Figure 1.6c). These genes are primarily involved in cell defense mechanisms, gene expression, and regulation. ALS pathogenesis can occur by specific mutations in genes. An expansion of a noncoding GGGGCC in C9orf82, D90A in SOD1, and S513P in FUS are the most well-known

mutations observed in ALS (Siddique and Siddique, 2021; Mejzini *et al*., 2019). Mutations on those genes can result in aggregation of toxic proteins which promote oxidative stress, mitochondrial dysfunction, and impaired axonal transport in neurons (Figure 1.6c) (Bonafede and Mariotti, 2017).

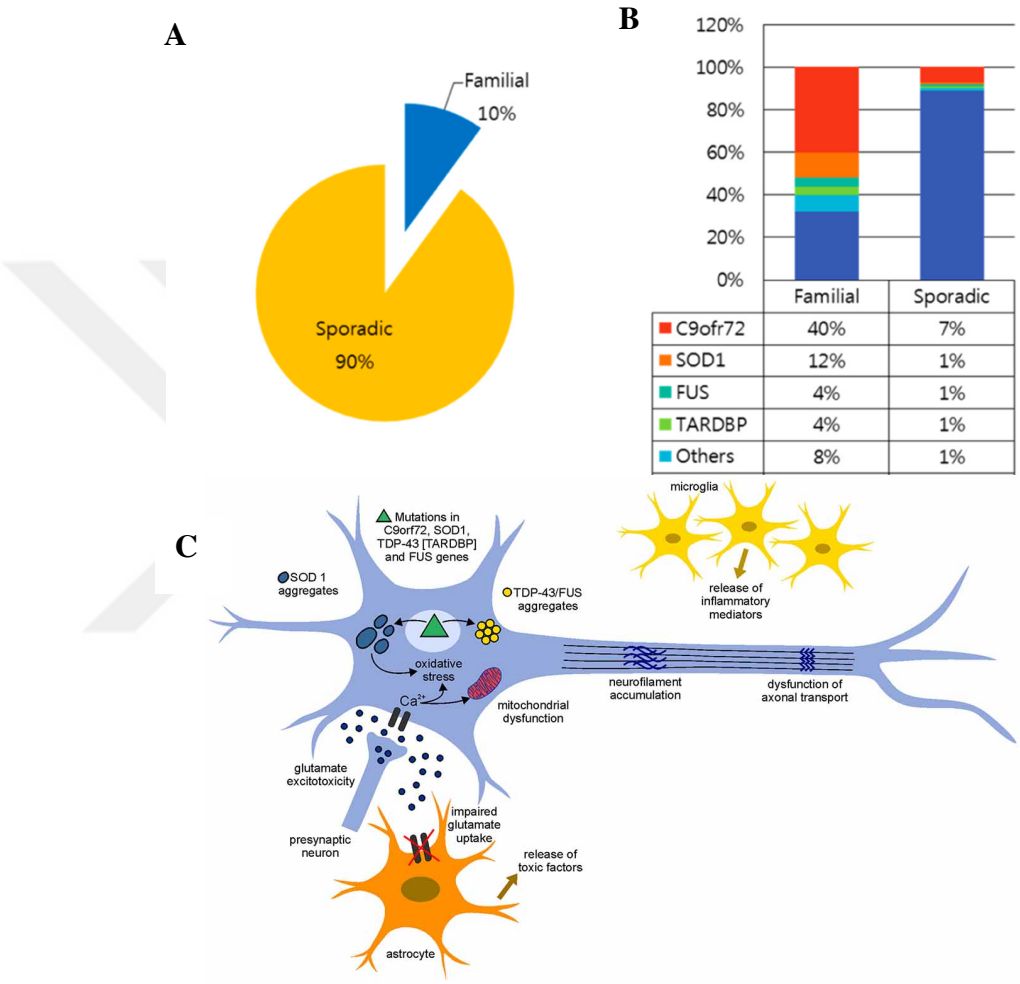

Figure 1.6. ALS disease types and responsible genes. (a and b) Distribution of type of ALS disease (a) and percentage of responsible genes (b). C9ofr72 was found the major responsible gene in fALS, but the cause of sALS is not still known. (Yun and Ha, 2020). (c) Effect of responsible genes on neurodegeneration in ALS disease (Bonafede and Mariotti, 2017).

To shed light on the ALS disease and to discover potential therapies, an international collaborative project called MinE was initiated to analyze whole-genome sequence data from at least 15.000 ALS patients, including control groups. By undertaking such a massive project, they sought to determine the abundance and distribution of genetic variations between patients (van Rheenen *et al*., 2018). Furthermore, a database would provide a plethora of information about the properties and mutations of ALS-related genes (van der Spek *et al*., 2019).

1.7. Nek1 in ALS Pathogenesis

NIMA (never in mitosis gene a)-related kinase 1 (NEK1) is one of the Ser/Thr kinase family members of NEK that shares a similar kinase domain. It is a 1258 aa length protein and contains an N-terminal kinase domain, predicted coiled-coil (CC) regions, a nuclear localization signal (NLS), and two nuclear export signals (NES) (Figure 1.7) (Melo-Hanchuk *et al*., 2017; Monroe *et al*., 2016) Due to the presence of both NLS and NES in the structure, it can traffic between the nucleus and cytoplasm, but is generally localized in the cytoplasm. In case of DNA damage, it translocates into the nucleus and activates the checkpoint kinases (CHK1 and CHK2) (Y. Chen *et al*., 2008; Feige *et al*., 2006).

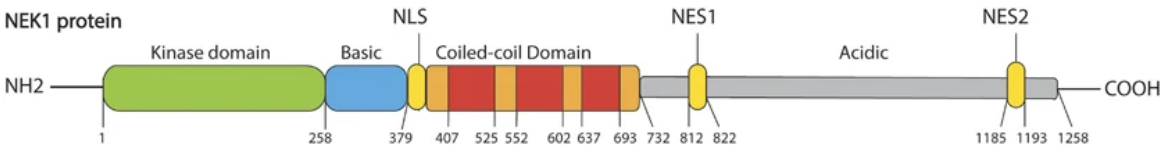

Figure 1.7. The domain structure of NEK1 protein (Monroe *et al*., 2016).

Nek1 has several functions in cellular processes such as mitosis, cell cycle regulation, DNA damage repair (DDR), and ciliary formation (Yao *et al*., 2021). Since Nek1 plays crucial roles in many cellular processes, it is also associated with various diseases. For example, point mutations on *Nek1* were found in patients suffering from spondylometaphyseal dysplasia (SMD) (Z. Wang *et al*., 2017). Loss of function mutations of *Nek1* can cause defects in embryogenesis, which leads to polycystic kidney disease (PKD) (Upadhya *et al*., 2000). Moreover, mutations in the kinase domain of *Nek1* are associated with short rib polydactyly

syndrome (SRP) (Upadhya *et al*., 2000). Recently, according to whole-exome analysis, John E. Landers and his colleagues found that loss of function of *Nek1* variants confer susceptibility to fALS (Kenna *et al*., 2016).

Whole-exome sequencing reports showed that 3% of ALS patients carry *Nek1* mutations (Table 1.1). Both loss of function and missense mutations significantly increase the risk of ALS disease. On the one hand, loss of function mutations in *Nek1* cause defects in neuronal morphology, neurite outgrowth, and microtubule dynamics in neurons leading to neurodegeneration. On the other hand, missense mutations promote protein aggregation in neurons and eventually loss of interaction with their partners (Yao *et al*., 2021).

Table 1.1. Some mutations of *Nek1* that observed in ALS patients (Brenner *et al*., 2016). The mutation considered in this study were indicated with asterisk.

Mutation	**Mutation type**	**Region**
nonsense	p.Ser14Ter	Kinase domain
nonsense	p.Arg812Ter*	NES
nonsense	p.Ser1036Ter	Acidic
missense	p.Asn181Ser	Kinase domain
missense	p.Arg261His	Basic
missense	p.Ala341Thr	Basic
missense	p.Gly399Ala	CC1
missense	p.Met545Thr	CC2
missense	p.Val704Ile	CC4
missense	p.Asn745Lys	CC4
missense	p.Val713Met	Acidic

1.8. A NEK1 Mutant Drives ALS pathogenesis

To elucidate how the p.Arg812Ter mutation affects ALS pathogenesis, a previous lab member Harun Öztürk generated a *Nek1* variant having this mutation, hereafter called truncated NEK1 (tNEK1). Since tNek1 had lost two NES sequences, it was found that, as expected, tNEK1 was trapped in the nucleus, contrary to mostly cytoplasmic localization of NEK1 (Figure 1.8a). Additionally, he also observed some aggregate-like structures of tNEK1 in the nucleus. As a characteristic feature of aggregates, a significant loss of solubility of tNek1 was observed (Figure 1.8b) (Öztürk, 2015).

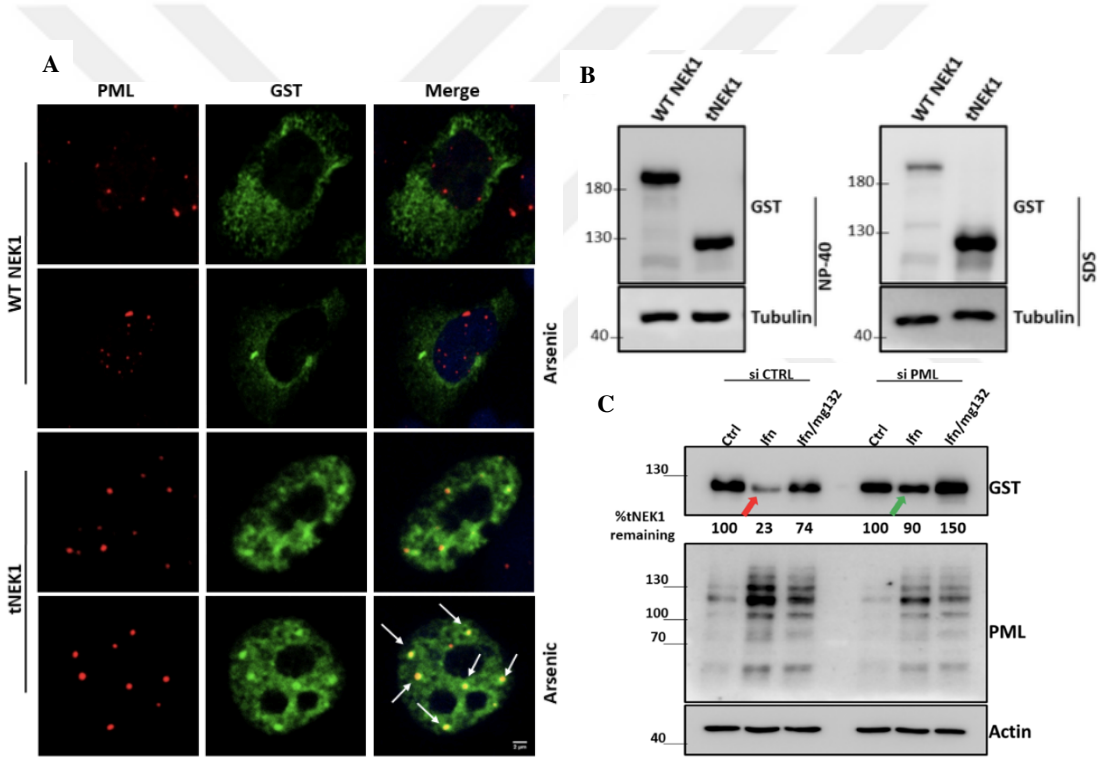

Figure 1.8. Aggregation and PML localization of pathogenic form of truncated NEK1 (tNEK1). (a) While wt NEK1 localizes at cytoplasm, tNEK1 localizes in the nucleus and aggregation-like structures were observed. (b) Like aggregated proteins, tNEK1 also resides in insoluble part of the lysate. (c) PML facilitates degradation of tNEK1.

It was known that sumoylation affects protein solubility and stability and is involved in neurodegenerative diseases, including ALS (Table 1.2). For instance, sumoylation of α-synuclein stabilizes and enhances protein aggregation, contributing to the development and

progression of Parkinson's disease (Yau *et al*., 2020). In addition, SUMO modification of ALS-related proteins such as SOD1, TDP43, and CTE (COOH terminus of EAAT2) is related to ALS pathogenesis (Dangoumau *et al*., 2013). In our laboratory, sumoylation of NEK1 and hypersumoylation of tNEK1 were demonstrated by our lab member, Bahriye Erkaya. Since misfolded proteins can be transferred PML NBs and get sumoylated, Harun postulated that tNEK1 might localize in PML NBs (Figure 1.8c). Pretreatment of cells with Arsenic trioxide (As) or Interferon-α (IFN), which induces PML NB nucleation and promotes recruitment of target proteins as previously described, caused full recruitment of tNek1, not Nek1, to PML NBs. These results show that tNek1 is an aggregation-prone misfolded protein that may undergo sumoylation in PML NBs. Further, PML NB-directed degradation of tNek1 was observed when cells were treated with IFN. This constitutes a promising finding for a potential targeted therapy for ALS disease.

Table 1.2. ALS-related proteins and their potential SUMO consensus sites (Dangoumau *et al*., 2013).

Genetic subtype	**Gene**	**Location of potential SUMO consensus sites (Position of lysine)**
ALS1	Superoxide dismutase (SOD1)	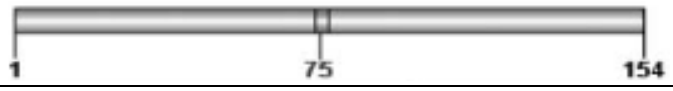
ALS6	Fused in sarcoma (FUS)	
ALS9	Angiogenin (ANG)	
ALS10	TAR DNA-binding protein (TARDBP)	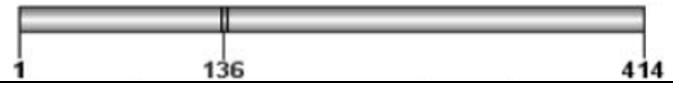
ALS12	Optineurin (OPTN)	
ALSX	Ubiquilin 2 (UBQLN2)	

1.9. Generation of a New Mouse Model

To study the effects of tNEK1 *in vivo*, we generated a C57BL/6 mouse expressing homozygous and heterozygous mutants of tNEK1. After successive breeding, homozygous mutant individuals of tNEK were also acquired. Several animal groups are being currently studied to investigate the impact of this mutation *in vivo*. There is a follow-up of lifespan study for different mice groups. Moreover, several motility assays are being performed weekly, which will help potential movement defects, pathological effects, and ALS-related symptoms found in these genetically modified, only tNEK1-expressing mice to be collected and recorded. Understanding the effects of tNEK1 *in vivo* is crucial, because it would allow the investigation of IFN treatment for ALS disease in preclinical mice models. For example, preliminary data showed that tNEK1 mutant carrying mice have a shorter lifespan and lower weight compared to their wildtype mice counterparts (Georgiadou, unpublished data). Walking disorders were investigated by standardized tests in the literature, like footprint and walking tests for motor neuron diseases such as Alzheimer's and Parkinson's diseases (Brooks and Dunnett, 2009; Rial *et al*., 2014; Sutoko *et al*., 2021).

In vitro studies showed that PML NBs are crucial for the clearance of pathogenic tNEK1 aggregates, and IFN-directed potential therapy is related to PML NB biogenesis. To investigate the effects of PML NB-targeted IFN treatment, we also generated a $PML^{-/-}$ mouse expressing homozygous and heterozygous tNEK1 mutations. Consequently, performing tests on these transgenic animals may provide information for a potential therapy for ALS disease.

1.10. Sumoylation of Non-eukaryotic Proteins

Although sumoylation occurs in eukaryotes, sumoylation of non-eukaryotic proteins is also documented in the literature. To give an example, viral proteins such as Rep78 of the AAV virus, E2 of the HPV virus, E1A of adenovirus and integrase of the HIV-1 virus, and a bacterial protein; TRP120 of *E. chaffeensis* are reported (Table 1.3) (Ribet *et al*., 2010; Wilson, 2017). The effects are also various; it can directly or indirectly stabilize the protein,

increase sumoylation of specific targets and function as STUbLs. It seems that sumoylation can be used as a defence mechanism against invaders or the invaders may use this mechanism for their benefits. For instance, when *Listeria monocytogenes* invades a host, a bacterial virulence factor, listeriolysin O (LLO), triggers the degradation of Ubc9 and some other sumoylated proteins, which results in immunosuppression.

Table 1.3. DNA viruses and their relation with sumoylation. Adapted from Springer (Wilson, 2017).

DNA Virus family	Virus	Protein	Sumo sites*	SIMs	Effect of sumoylation or effect on sumoylation system
Parvovirus	AAV	Rep78	K84	-	Sumoylation may stabilize Rep78
Papillomavirus	HPV	E1	K559	-	Role of sumoylation unclear
		E2	K292	-	Sumoylation indirectly stabilizes E2
		E6	-	-	Blocks sumoylation of PIASy substrates; Degrades Ubc9
		E7	-	-	Inhibits sumoylation of pRB
		L2	K35	+	Modulate L2 incorporation int capsids
Adenovirus	Ad5	E1A	-	-	Blocks pRB sumoylation; binds Ubc9
		ElB-55K	K104	-	SUMO E3 ligase
		E40rf3	-	-	Increases sumoylation of specific targets
Herpesvirus	HSV	ICP0	-	+	STUbL
	VZV	ORF29p	+	-	Role of sumoylation unknown
		OFR61	-	+	Possible STUbL
	CMV	IE1	K450	-	Sumoylation prevents binding to STAT2
		IE2-p86	K175/K180	+	Sumoylation enhances transactivation activity
		UL44	Multiple	-	Sumoylation enhances DNA binding
		pp71	-	-	Increases sumoylation of Daxx

On the other hand, SUMO overexpression shows protection from bacterial infection (Ribet *et al*., 2010). In addition, a recently published study from our lab shows that HIV

type-1 impairs global sumoylation by targeting SUMO E1-activating enzymes. Impairment of sumoylation is suggested to prevent immune defense mechanisms, such as T-cell expansion and activity, thus contributing to the development of the disease (Mete *et al*., 2022). These findings show that sumoylation is an essential modification that affects host-pathogen interactions.

1.11. A Bacterial Adaptive Immune Defence Mechanism: CRISPR

Clustered Regularly Interspaced Palindromic Repeats (CRISPR) is a bacterial and archaeal adaptive immune mechanism against viral infection (Figure 1.9). In case of a second invasion, a quick and robust response occurs, (1) transcription of the CRISPR locus containing repeats that are called Pre-CRISPR RNA, (2) maturation of CRISPR RNA by cleaving each repeat sequence to separate spacers and complex formation with RNAse, trans-activating RNA (tracrRNA) and Cas9, and (3) DNA targeting via spacer if PAM sequence is present in viral DNA (will be explained later), and finally (4) viral DNA cleavage (Mali *et al*., 2013).

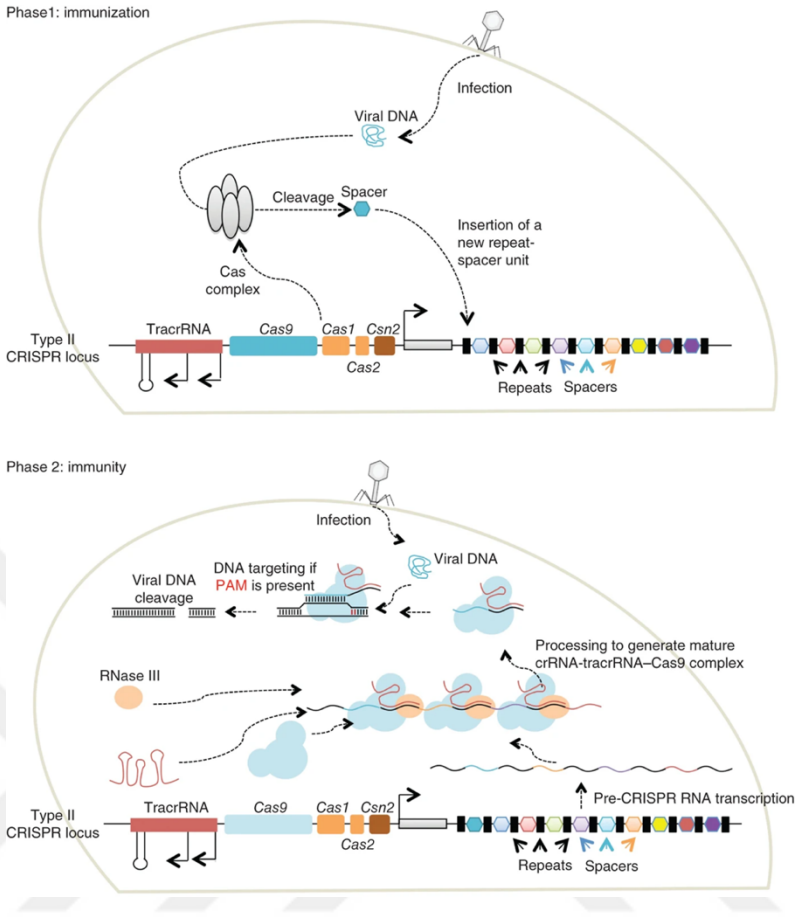

Figure 1.9. Cas9-related bacterial immune mechanism. Reprinted by permission from Springer Nature.

Protospacer Adjacent Motif (PAM) is an essential component that prevents the CRISPR locus itself from being targeted. PAM sequence varies between species, such as NGG for *S. pyogenes* and NGGNG for *S. thermophiles* (N: any nucleotide). Other than that, the PAM sequence also provides specificity for the recognition of foreign DNA. For example, long PAM sequences, like NGGNG, are more specific than short PAM sequences like NGG; however, it becomes harder to target the DNA with long PAM sequences (F. Zhang *et al.*, 2014).

Two classes of CRISPR/Cas systems exist based on the structure and function of Cas; class I and class II. They are also subdivided into different types. Some of these types recognize and cleave DNA (e.g., type II of class II), edit RNA (e.g., type VI of class II), and edit both DNA and RNA (e.g., type III of class I). It should be noted that type II and V from

the class II system are primarily seen in bacteria. Also, the type II CRISPR/Cas9 system belonging to *Streptococcus pyogenes* has been developed for gene-editing technologies (Liu *et al*., 2020). The diversity among different types of CRISPR systems allows development of new applications in gene editing mechanisms, which will be mentioned later.

1.12. Cas9 and Cleavage of DNA

In order to understand the CRISPR/Cas mechanism, the structure of Cas9 should be examined. Cas9 is a large protein of about 160kDa consisting of two catalytic nuclease domains; HNH and RuvC, a PAM-interacting domain, and a Recognition (REC) lobe for interaction with nucleic acids. When the crRNA-tracrRNA-Cas9 complex attaches to a target gene via the PAM-interacting domain of Cas9, base-pairing occurs between the spacer sequence of crRNA and a single strand of target DNA (Figure 1.10). Then, HNH and RuvC domains generate double-strand breaks on target DNA by cleaving the crRNA-matched strand and the opposite strand, respectively (Jiang and Doudna, 2017).

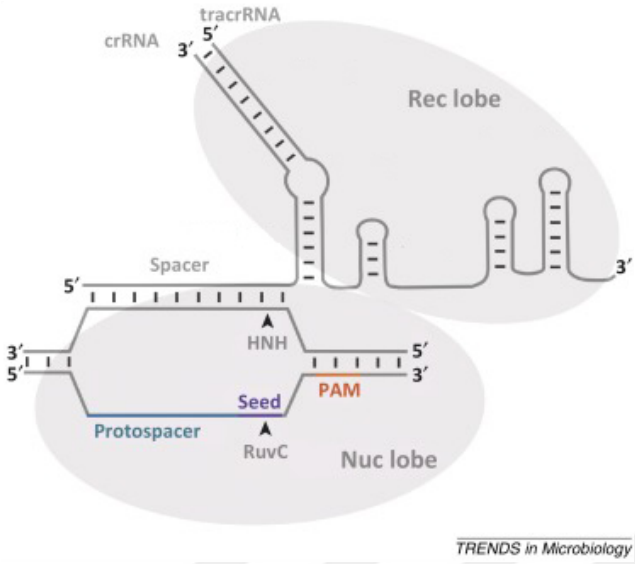

Figure 1.10. Structure of DNA binded crRNA-tracrRNA-Cas9 complex. Reprinted from Trends in Microbiology with permission from Elsevier.

1.13. Developments in Gene Editing Technology

The discovery of the CRISPR/Cas system in bacteria has a significantly positive impact on biological sciences, since it was soon adapted to genome editing technology. Previously, some artificial genome editing techniques such as Zinc-finger nucleases (ZFNs) and transcription activator-like effector nucleases (TALENs) were developed. However, they were rather challenging to apply and proved to have disadvantages compared to CRISPR/Cas system. For example, the recognition of target DNA guided by a protein, like in ZFN, had low specificity because amino acids can recognize different combinations of codon sequences. Additionally, RNA-guided Cas9 requires Watson-Crick base pairing between spacer sequence and target DNA (H. Wang *et al*., 2016). For these reasons, CRISPR/Cas9 system has been developed for gene editing and becoming particularly used in many studies (C. Zhang *et al*., 2018).

One of the most critical developments in the CRISPR/Cas9 system is its simplification by the generation of a chimeric RNA with tracrRNA and crRNA, which is called guide RNA (gRNA), and it has become the most widely used system for gene editing. An editable ~20

nucleotide sequence in gRNA allows targeting of any DNA sequence containing PAM by binding to both Cas9 and the target DNA sequence (H. Wang *et al*., 2016). To make the CRISPR/Cas9 system compatible with eukaryotes, additional changes/innovations were made. Since every organism uses different codon sequences to express a protein, an optimization in the Cas9 sequence is required to achieve compatibility in usage for the desired organism. Besides, NLS was added at the beginning of the N- or C-terminus on both ends of the Cas9 sequence to be imported to the nucleus (Mali *et al*., 2013).

Gene editing by CRISPR/Cas9 was made by DNA repair mechanisms. After double-strand breaks occur in target DNA, the error-prone nonhomologous end-joining (NHEJ) mechanism starts to repair if no template exists for the repair process (Figure 1.11a). The nature of the mechanism is not very specific since nucleotides are added randomly. Consequently, some insertions, deletions, or frameshift mutations can occur in a cleaved site, which generally results in disrupted or abolished gene function. If the target gene does not function anymore, the null allele is called knock-out (KO). Making KO of desired genes provides an opportunity to investigate the physiological relevance, importance, and functionality of those genes (Lo and Qi, 2017).

However, if there is a template DNA, the homology-directed repair (HDR) mechanism starts to repair double-strand breaks by considering the template DNA (Figure 1.11a). This mechanism allows insertions for desired genes, called knock-in (KI); deletions, called knock-out (KO), and corrections or mutations in target DNA. It should be noted that HDR generally occurs in the G2/S phase of the cell cycle, which is the most active phase. The advantage of this technique rather than NHEJ is the opportunity to control mutations in the desired way and elimination of unwanted mutations (Jasin and Rothstein, 2013). The drawback of HDR is its low efficiency for gene editing, which is about 10%. Also, it is a very time-consuming process, taking at least 24 days. To overcome these problems, one of the nuclease domains of Cas9 was mutated; D10A for RuvC or H840A for HNH domains, creating Cas9 nickase (nCas9) (Figure 1.11b). It was shown that nCas9 creates single-strand breaks that get repaired in a shorter time, reducing the process down to 9 days while increasing the efficiency of gene editing (Liu *et al*., 2020; Ma *et al*., 2014).

To open up new areas in CRISPR genome editing technology, Cas9 was modified by mutations or some proteins and reporters were added. For instance, the nuclease activity of Cas9 was depleted entirely by mutating both nucleases by introduction of the D10A mutation in RuvC, and H840A mutation in HNH nuclease domains, creating catalytically dead Cas9 (dCas9). This mutation can bind to its target directed by gRNA, but cannot cleave it. In this way, DNA binding efficiency can be detected by Chromatin Immunoprecipitation (ChIP). In addition, the fusion of Cas9 with some proteins or molecules can change the use of the application of CRISPR (Figure 1.11c and d). For example, gene expression can be increased or decreased by fusion with transcriptional activation or repression domains, and histone modifications can change the epigenome. The target gene's activity can be altered when dCas9 is fused with histone methylases, or DNA methyltransferases which cause silencing, or with histone acetyltransferases and DNA demethylases which cause re-activation of the gene (Lo and Qi, 2017).

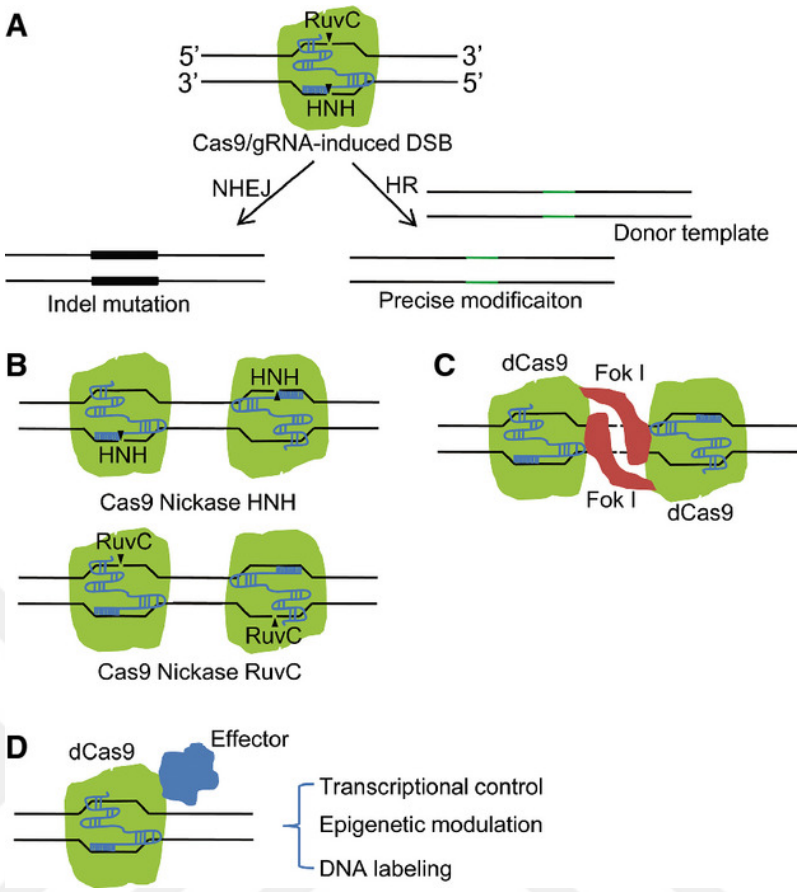

Figure 1.11. Usage of different types of CRISPR/Cas9 systems. (A) In normal scenario, Cas9/gRNA- induced double strand breaks are repaired by nonhomologous end joining (NHEJ) and homology directed repair (HR) mechanisms. (B,C and D) This technology has developed to increase usage areas (Ma *et al*., 2014).

The fact that Cas9 can also bind other sites on the genome that has a PAM sequence rather than the target site can lead to unwanted results, some studies were focused on increasing on-target and decreasing off-target activity by editing Cas9. For instance, Slaymaker and his colleagues hypothesized that positively charged amino acids in HNH, RuvC, and PAM-interacting domains of Cas9 might interact with negatively-charged DNA. They found that some combinations of mutants on critical residues (K810A/K1003A/R1060A and K848A/K1003A/R1060A), called enhanced Cas9 (eCas9), resulted in decreased off-target effects while on-target activity remained the same (Slaymaker *et al*., 2016). Thus this finding creates an opportunity for the improvement of Cas9.

1.14. Discovery of SUMO and Ubiquitin Modifications of Cas9

In our lab, PTMs of Cas9 by SUMO and Ubiquitin were discovered by previous lab members (Celen, 2019) He demonstrated them by performing Immunoprecipitation (IP), His-pulldown, and Proximity Ligation Assay (PLA) experiments. Ubiquitylation of Cas9 was also found by Mass Spectrometry (MS/MS), and the assay revealed 14 ubiquitylation sites. Based on these findings, in this study, we aimed to find the effects of SUMO modification on the Cas9 protein. We tested its turnover rate, crosstalk with Ubiquitin, and DNA binding ability.

2. AIM OF STUDY

The major aim of this study is to show that pathogenic tNEK1 aggregates are cleared from cells following hypersumoylation and ubiquitylation, in a PML-dependent manner, in particular, upon exposure to interferon-α. In addition, we aim to document some of the pathological outcomes in a novel mouse model that expresses tNEK1, by performing walking assays – as a readout for motor neuron function. We expect that these findings will eventually help us to research a potential treatment for ALS in preclinical models. Additionally, we sought to identify Cas9 sumoylation site(s) and the effects of sumoylation on Cas9 function.

3. MATERIALS

3.1. Cell Culture and Mouse Studies

HEK293 cells were kindly provided by Prof. Dr. Nurhan Özlü from Koç University and SH-SY5Y cells were given by Prof. Dr. Aslı Tolun from Istanbul Technical University. BALB/C mouse models were donated by Prof. Dr. Hugues De Thé from College de France. GFP-stable HEK293 cells were provided by Prof. Dr. Tamer Önder from Koç University.

3.2. Plasmids, Primers and siRNAs

Plasmids used in this study are listed in Table 3.1. The following table represents primers and siRNA sequences (Table 3.2).

Table 3.1. Plasmids.

Construct	Origin	Backbone
GFP-SUMO1	Provided by Dr. Hugues De Thé, College de France	pcDNA3.1
GFP-SUMO2	Provided by Dr. Hugues De Thé, College de France	pcDNA3.1
GFP-Ubc9	Provided by Dr. Hugues De Thé, College de France	pcDNA3.1
His-Ubiquitin	Provided by Dr. Hugues De Thé, College de France	pcDNA3.1
pCW-FLAG-Cas9	Addgene, USA	pCW
pCW-Flag-dCas9	Provided by Dr. NC Tolga Emre, Boğaziçi U.	pCW
pEBG GST-NEK1 tv1	Provided by University of Dundee, DU41359	pEBG

Table 3.1. Plasmids (cont.).

Construct	Origin	Backbone
PLKO5-sgIRF4-KO1	Provided by Dr. NC Tolga Emre, Boğaziçi U.	PLKO5
PLKO5-sgPS2-ERE3	Provided by Dr. NC Tolga Emre, Boğaziçi U.	PLKO5

Table 3.2 Primers and siRNAs.

Primer	Sequence (5'-3')	Application
IRF4-KO1-test2F	GGTGTGGGAGAACGAGGAGA	qPCR
IRF4-KO1-test2R	GTTGTAGTCCTGCTTGCCCG	qPCR
pS2-ERE- test-4F	GCCTAGACGGAATGGGCTTC	qPCR
pS2-ERE- test-4R	AGAGATGGCCGGAAAAAGGC	qPCR
siCTRL	UUCUCCGAACGUGUCACGUTT	Silencing
siPML	AAGAGTCGGCCGACTTCTGGT	Silencing

3.3. Equipment and Devices

Equipment used in this study are listed in Table 3.3. The following table presents devices used in this study (Table 3.4).

Table 3.3. Equipments.

Name	Supplier
Cell Culture Dishes (60 mm, 100mm)	TPP, Switzerland
Cell Culture Flasks (75cm^2)	TPP, Switzerland
Cell Scraper	TPP, Switzerland
Cryovial Tubes (2ml)	CAPP, Denmark
Dynabeads Protein G	Thermo Scientific, USA

Table 3.3. Equipments (cont.).

Name	Supplier
Microfuge Tubes	CAPP, Denmark
Multiwell Plates	TPP, Switzerland
Nitrocellulose Blotting Membrane (0.2um)	GE Life Sciences, England
Petri Dishes	Fırat Plastik, Turkey
Pipette Tips (Filtered)	BioPointe Scientific, USA
Pippette Tips (Bulk)	CAPP, Denmark
Protein A Resin Captiva	Repligen, USA
Syringe Filter Units (0.22 μm, 0.45 μm)	EMD Millipore, USA
Syringes (1ml, 5ml, 10ml, 50ml)	Set Medikal, Turkey

Table 3.4. Devices.

Device name	Brand
Autoclaves	Midas 55, Prior Clave, UK AS260T, Astell, UK
BD Accuri	BD, USA
Carbon dioxide tank (cell culture)	Genç Karbon, Turkey
Cell culture incubator	WTC, Binder, Germany
Centrifuges	Allegra X-22, Beckman Culture, USA
Cold room	Birikim Elektrik Soğutma, Turkey
Confocal microscope	Leica SP8, USA
Documentation system	Gel Doc XR system, Bio-Doc, USA
Dynabead stand	ThermoFisher, USA
Fluorescent microscope	Axio Observer.Z1, Zeiss, Germany
Freezers and refrigerators	4 °C: Uğur, USS 374 DTKY, Turkey -20 °C: Uğur, UFR 370 SD, Turkey -80 °C: ULT deep freezer, Thermo, UK

Table 3.4. Devices (cont.).

Device name	**Brand**
Heat block	Block Heater Analog, VWR, USA
Ice flaker	AF20, Scotsman Inc., Italy
Laminal flow cabinet	Class IIB, Tezsan, Turkey
Micropipettes	Finnpipette, Thermo, USA
Microwave oven	Arçelik, Turkey
Nanodrop	ND-1000, Thermo Fisher, USA
Oven	Gallenkamp, 300, UK
pH meter	Hanna Instruments, USA
Pipettor	S1 Pipet Filler, Thermo Fisher, USA
Power supply	EC XL 300, Thermo Fisher, USA
PikoReal Real-Time PCR system	Thermo Fisher, USA
Rotator-mixer	Grant Instruments, UK
Shaker	Analog Orbital Shaker, VWR, USA
Software	ImageJ, NIH, USA PyMOL, USA Syngene-Genetools, UK Leica LAS X, USA
Sonicator	Sonoplus, Bandelin, Germany Q800, QSonica, USA
Vortex	Silverline, VWR, USA
Water purification	WA-TECH UP Water Purification Sys., Germany
Western blot documentation system	G-BOX Chemi XX6, Syngene, UK

3.4. Reagents, Kits, Enzymes and Chemicals

Reagents, kits and enzymes used in this study are shown at Table 3.5. Chemicals were described in Table 3.6.

Table 3.5. Reagents kits and enzymes.

Product	Supplier
ChIP DNA Clean & Concentrator	Zymo Research, USA
Complete Mini Protease Inhibitor Cocktail	Roche, Switzerland
DNA Ladder (1kb)	NEB, USA
Duolink® In Situ Detection Reagents Orange	Sigma-Aldrich, USA
Duolink® In Situ PLA® Probe Anti-Rabbit MINUS	Sigma-Aldrich, USA
Duolink® In Situ PLA® Probe Anti-Rabbit PLUS	Sigma-Aldrich, USA
ECL	Advansta, USA
HiPerFect Transfection Reagent	Qiagen, Netherlands
NucleoSpin Gel and PCR Clean-up kit	Machery-Nagel, Germany
Nucleospin MiniPrep Kit	Machery-Nagel, Germany
PageRuler Prestained Protein Ladder	Thermo, USA
RealQ Plus Master Mix	Ampliqon, Denmark
Sirius	Advansta, USA
ZymoPURE Plasmid MidiPrep Kit	Zymo Research, USA
dNTP mix	NEB, USA
Proteinase K	Jena Bioscience, Germany
RNase A	Thermo Scientific, USA

Table 3.6. Chemicals.

Chemical	**Brand**
2-mercaptoethanol	Merck, Germany
4'6-diamidino-2-phenylindole (DAPI)	Sigma-Aldrich, USA
Acetic acid	Sigma-Aldrich, USA
Acrylamide	Bio-Rad, USA
Ammonium persulfate (APS)	AppliChem, Germany
Ampicillin	Merck, Germany
Bromophenol blue	Sigma-Aldrich, USA
Calcium chloride dehydrate	Sigma-Aldrich, USA
cOmplete™, EDTA-free Protease Inhibitor Cocktail	Roche, Switzerland
Cycloheximide	Sigma-Aldrich, USA
Dimethyl sulfoxide (DMSO)	Sigma-Aldrich, USA
Doxycycline hyclate	Merck, Germany
Dulbecco's Modified Eagle Medium (DMEM)	Gibco, Fisher Scientific, USA
Ethanol	Merck, Germany
Ethylenediaminetetraacetic acid (EDTA)	Wisent Bioproducts, Canada
Fetal Bovine Serum (FBS)	Gibco, Fisher Scientific, USA
Glycerol	MP Biomedicals, USA
Glycine	NeoFroxx, Germany
HEPES buffered saline (HBS)	Lonza, Switzerland
Hydrochloric acid	Sigma-Aldrich, USA
Interferon-α (human)	Roche, Switzerland
Isopropanol	Sigma-Aldrich, USA
Kanamycin	Gold Biotechnology, USA
Luria-Bertani (LB) Agar	Caisson Laboratories, USA
Luria-Bertani (LB) Broth	Caisson Laboratories, USA

Table 3.6. Chemicals (cont.).

Chemical	Brand
Methanol	Merck, Germany
MG132	Calbiochem, Germany
ML792	Medkoo Biosciences, USA
N-ethylmaleimide (NEM)	Sigma-Aldrich, USA
Nonidet P-40	Sigma-Aldrich, USA
Paraformaldehyde (PFA)	Santa Cruz Biotechnology, USA
Penicillin/Streptomycin (100X)	Lonza, Switzerland
Phenol-chloroform-Isoamyl alcohol	Sigma-Aldrich, USA
Sodium chloride	Merck, Germany
Sodium Deoxycholate	Sigma-Aldrich, USA
Sodium dodecyl sulfate (SDS)	Merck, Germany
Sodium hydroxide	Merck, Germany
Technical Ethanol	Çakır Kimya, Turkey
Tetramethylethylenediamine (TEMED)	Sigma-Aldrich, USA
Tris-base	Biofroxx, Germany
Triton X-100	VWR, USA
Trypsin-EDTA (0,05%, 0,25%)	Gibco, Fisher Scientific, USA
Tween 20	Merck, Germany

3.5. Buffers and Antibodies

Buffers and their ingredients used in this study were shown in Table 3.7. Antibodies with their concentrations used in experiments were shown in Table 3.8.

Table 3.7. Buffers.

Buffer name	**Ingredients**
10X SDS Western blot running buffer	1% (w/v) SDS, 3.03% (w/v) Tris base, 11.41% (w/v) glycine in ddH_2O
10X SDS Western blot transfer buffer	3.03% (w/v) Tris base, 11.41% (w/v) glycine in ddH_2O
4X Laemmli buffer	200 mM Tris-HCl (pH 6.8), 8% SDS, 40% glycerol, 4% 2-mercaptoethanol, 50 mM EDTA, 0.08% bromophenol blue in ddH_2O
5% Stacking gel (Western Blot)	0.125 mM Tris-HCl (pH 6.8), 0.1% (w/v) SDS, 4% (w/v) acrylamide:bisacrylamide 0.05% (w/v) APS,0.0075% (w/v) TEMED in ddH_2O
8% Resolving gel (Western blot)	375 mM Tris-HCl (pH 8.8), 0.1% (w/v) SDS 8% (w/v) acrylamide: bisacrylamide 0.05% (w/v) APS, 0.005% (w/v) TEMED in ddH_2O
Immunoprecipitation (IP) lysis buffer	2% SDS, 50 mM Tris-HCl (pH 8.0), 20 mM NEM, Protease inhibitor cocktail, in ddH_2O
Ponceau stain	5% Glacial acetic acid, 0,1% Ponceau S, in ddH_2O
Radioimmunoprecipitation (RIPA) buffer	50 mM Tris-HCl, 250 mM NaCl, 1% NP-40, 10% glycerol, 0,1mM EDTA (pH:8) in ddH_2O (pH 7.4)
Western blot blocking & antibody solution	5% (w/v) non-fat dry milk in TBS-T
NEM Stock solution	0,5M NEM in EtOH
NEM Working solution	400ul NEM Stock in 10ml PBS

Table 3.7. Buffers (cont.).

Buffer name	Ingredients
Western Blot Membrane stripping buffer (mild)	7,5g Glycine, 0,5g SDS, 5ml Tween 20, pH:2,2
1X TBS-T	50mM Tris HCl pH:7.4, 150mM NaCl, 0,05% Tween-20
ChIP lysis buffer	50mM HEPES, 150mM NaCl, 1% Triton-X100 0,1% Na-deoxycholate, 1mM EDTA
ChIP nuclear lysis buffer	50mM Tris pH:8, 10mM EDTA pH:8, 1% SDS
ChIP dilution buffer	16,7mM Tris pH:8, 1,2mM EDTA pH:8, 0,01% SDS, 1,1% Triton-X 100
High salt (NaCl) buffer	50mM HEPES, 500mM NaCl, 1% Triton-X100 0,1% Na-deoxycholate, 1mM EDTA
LiCl buffer	100mM Tris pH:8, 500mM LiCl, 1% deoxycholic acid, 1% NP40
PBS-T	1X PBS, 0,05% Tween-20
1X TE buffer	10mM Tris pH:8, 1mM EDTA pH:8
IF Permeabilization buffer	0,05% TritonX-100 in 1X PBS
IF Blocking buffer	1% BSA in PBS-TX

Table 3.8. Antibodies.

Antibody	Supplier	Source	Dilution
FLAG (#F1804)	Sigma, USA	Mouse	WB (1:1000)
Cas9 (#844301)	BioLegend, USA	Mouse	IF (1:100)
β-Actin (#MA1115)	BosterBio, USA	Mouse	WB (1:1000)
FLAG (#14793S)	CST, USA	Rabbit	WB (1:1000) IF (1:400)
6X Histidine (#sc-57598)	Santa Cruz Biotech, USA	Mouse	WB (1:1000)

Table 3.8. Antibodies (cont.).

Antibody	Supplier	Source	Dilution
Mouse IgG, Alexa Fluor 546 (#A-11003)	Thermo Fisher Scientific, USA	Goat	IF (1:800)
Rabbit IgG, Alexa Fluor 488 (#A-11034)	Thermo Fisher Scientific, USA	Goat	IF (1:800)
SUMO1 (#4930S)	CST, USA	Rabbit	WB (1:1000) IF (1:300)
SUMO2/3 (#ab3742)	Abcam, UK	Rabbit	WB (1:1000) IF (1:2400)
Ubiquitin FK2 (#BML-PW8810-0500)	Enzo Life Sciences, USA	Mouse	WB (1:1000) IF (1:300)
GST (#26H1)	CST, USA	Mouse	WB (1:1000) IF (1:2000)
PML (#sc-377390)	Santa Cruz Biotechnology, USA	Mouse	WB (1:500)
PML (#sc-5621)	Santa Cruz Biotechnology, USA	Rabbit	IF (1:400)
Anti-Mouse IgG HRP (#7076S)	CST, USA	Goat	WB (1:1000)
Anti-Rabbit IgG HRP (#7074S)	CST, USA	Goat	WB (1:1000)

4. METHODS

4.1. Cell Culture

HEK293 cells were maintained in Dulbecco's Modified Eagle Medium (DMEM) containing 10% Fatal Bovine Serum (FBS) and 1% Penicillin/Streptomycin. They were grown in 75mm^2 cell culture flasks and incubated at 37°C and 5% CO_2. When the confluency was reached at approximately 90%, cells were passaged by following steps: discarding medium, washing cells with PBS, incubation with trypsin for 5 min at 37°C, deactivation of trypsin with DMEM, and seeding of the cells with the amount of 60.000cells/mm^2 into new flasks. Passaging occurs every 2-3 days.

To store cells for greater extended usage, cells were collected in a freezing medium containing 20% FBS and 10% DMSO and were aliquoted into cryovial tubes, stored at -80°C overnight, and placed at -150°C for more extended storage. To defrost cells, cells were resuspended in 5ml of complete medium and centrifuged for 3min at 300 x g. Then, the pellet was resuspended and cultured into flasks.

4.2. Treatments

For NEK1 assays, HEK293 and SH-SY5Y cells were treated with human Interferon-α (1000U) for 48h. To induce Cas9 expression on pCW-Cas9 plasmid and Cas9-stable HEK293 cells, doxycycline (2μg/ml) was given directly into the cell medium a day before the experiment.

MG132 was added to the cell medium with 10μM for 6h, or 2μM overnight before the beginning of the experiment. Since MG132 is diluted in DMSO solution, control cells were treated with the same volume of DMSO as a mock. Cells were pre-treated with ML792 (1μM) for 24h.

4.3. Transfection

The transfection of HEK293 cells was performed the day after cell seeding when the confluency reached 50-70%. For 10cm cell culture dishes, 15-20ug DNA in 438 µl ddH_2O was mixed with 62µl 2M Calcium Chloride ($CaCl_2$) dropwise and incubated at room temperature for 5min. After incubation, ice-cold 2X HBS solution was added to the mixture dropwise, mixed well, and incubated at room temperature for 10min. Finally, the mixture was resuspended and distributed to cells in a dropwise manner.

4.4. siRNA transfection

For siRNA transfection, 0,4-1,6x10^5 cells were seeded on 24 well plates and were put in an incubator. To prepare the siRNA mixture, 20µM siRNA was diluted in 100µl of incomplete DMEM. Then, 3µl of HiperFect solution was added to diluted siRNA and was mixed by vigorously After 5-10min incubation at room temperature, the transfection mixture was given to the attached cells. The next day, DNA transfection was performed. As a negative control, control siRNA (siCTRL) was used.

4.5. Immunoprecipitation (IP)

IP was performed on 10cm cell culture dishes after 18-24 hours of transfection. First, the medium was discarded and 1ml ice-cold NEM Working Solution was given to cells and incubated for 3min on ice. After the solution was discarded, 5ml ice-cold PBS was given to cells. Cells were scraped and collected in a falcon tube and were centrifuged at 300 x g for 5min at +4°C. Supernatant was removed, and the pellet was resuspended in 120-150µl IP Lysis Buffer containing Protease Inhibitor Cocktail (PIC). The lysate was sonicated by Bandelin SonoPlus (amplitude 60%, 15sec, 8 cycles) twice or until the lysate got homogenous and clear. Sonicated lysate was 1:10 diluted with RIPA containing PIC and centrifuged at 15000rpm for 30min at +4°C. Meanwhile, protein A agarose beads were equilibrated by washing 5-6 times with RIPA. After the centrifugation, the supernatant was transferred into

two tubes; 45µl of the solution was mixed with 15µl 4X Laemmli buffer and stored at -20°C, and the remaining was precleared with 25µl equilibrated beads on a tube rotator at room temperature for 45 minutes. Next, the lysate was spun down for 1 minute and transferred to a new 1.5ml microfuge tube to get rid of beads, and 2µg of antibody was added to the lysate and incubated for 1.30h at +4°C on rotation. Later, 50µl of equilibrated beads was added to the lysate for 1.30h at +4°C on rotation. After the incubation, the lysate was spun down for 1 minute; the supernatant was carefully removed. Antigen-bound beads were washed three times with ice-cold RIPA and one time with ice-cold PBS, and all the liquid was aspirated using an insulin syringe. Finally, beads were resuspended in 40-75µl of 2X Laemmli buffer, boiled at 95°C for 10min, spun down for 1min, and stored at -20°C.

4.6. Chromatin Immunoprecipitation (ChIP)

Before starting ChIP, cells on a plate were counted, which is essential for the procedure. First, to fix the DNA-protein complex, formaldehyde (final concentration: 1%) was added to the 10cm plate and incubated for 10min on a shaker at 170rpm. Then, glycine (final concentration: 0,125 M) was added to the plate and incubated for 5min on a shaker to stop the crosslink reaction.

Second, for cell lysis, cells were scraped on ice, collected on 50ml falcon tubes, and centrifuged at 2000rpm, for 2min at +4°C, and the supernatant was removed. Pellet was washed twice with ice-cold PBS and centrifuged for 2min, 2000 rpm at +4°C. Then, the pellet was resuspended with cellular lysis buffer containing Protease Inhibitor Cocktail (PIC) (1ml buffer per $10x10^6$ cells) and incubated for 5min on ice and centrifuged for 2min, 1200rpm at +4°C, and the supernatant was discarded. Next, the pellet was resuspended in NLB containing PIC, 300µl of buffer per $10x10^6$ cell. Resuspended nuclei were aliquoted into 0,5ml thin-wall PCR tubes, 300µl in each tube, and sonicated at the following conditions: 60% amplitude, 15sec on, 45sec off, total time 80min at +4°C. Sonicated lysates were centrifuged for 10min, 14.000rpm at +4°C, and supernatants from the same samples were collected into a new tube.

Third, magnetic beads were prepared for ChIP by taking 25µl of Dynabead Protein-G magnetic bead per single IP and washed twice with 0,5ml of PBS-T. 2,5µg of antibody was added to 25µl of bead diluted in 150µl of PBS-T for each IP, and incubated 45-60min at room temperature, rotating on an orbital shaker. After the pre-binding of the antibody, beads were washed twice with 0,5ml PBS-T and 0,5ml IP dilution buffer containing PIC and re-suspended with IP dilution buffer containing PIC to make the initial volume. Next, chromatin lysate was 1:10 diluted with IP dilution buffer containing PIC in 2ml protein LoBind® tubes (Eppendorf). Meanwhile, 150µl of cell lysate was placed in another tube as an input. Anti-body-bound beads were mixed with cell lysate and incubated for 1h at room temperature, rotating on an orbital shaker.

Fourth, immune complex bound beads were washed twice with 0,75-1ml IP dilution buffer (x2), high salt CLB buffer, LiCl buffer, and TE buffer (x2), respectively. After the washing, beads were resuspended in 100µl of TE buffer and transferred to a clean 1,5ml tube. To recover DNA, RNaseA (final concentration: 0,1µg/µl) was added to the input and incubated for 1h at 38°C. Then, inputs and IP samples were boiled for 10min at 95°C and cooled down on ice. After that, Proteinase K (final concentration: 200ng/µl) was added to inputs and IP samples, and incubated for 30 min at 55°C. After incubation, inputs and IP samples were boiled for 10min at 95°C and cooled down on ice. Later, IP samples were transferred to new tubes to get rid of beads. Finally to purify DNA from the input and IP sample, the phenol-chloroform extraction method was performed, and DNA was resus-pended in 1X TE buffer with the volumes of 25µl for input and 20µl for IP sample.

4.7. Phenol/Chloroform DNA Isolation

To isolate the DNA from IP and input samples of the ChIP experiment, they were mixed with an equal volume of phenol/chloroform/isoamyl alcohol in the fume hood. The mixture was centrifuged for 5min at 14.000 x g, and the upper phase of the solution was transferred to new microfuge tubes, but avoiding taking the lower phase. After that, 2X vol-ume of 100% EtOH, 0,1X volume of 3 M sodium acetate, and 1µl of glycogen was mixed

with the sample and incubated at -80°C for at least 30min. Next, samples were centrifuged for 10min at max speed, at +4°C, and the supernatant was removed. The pellet was washed twice with 1ml of ice-cold 70% EtOH and centrifuged for 5min at max speed, at +4°C. Then, EtOH was removed, and the pellet was allowed to dry at 50°C for about 1h. Finally, the DNA pellet was resuspended in sterile 1X TE buffer or ddH_2O.

4.8. Quantitative Polymerase Chain Reaction (qPCR)

qPCR reaction was used for the ChIP experiment with the dilutions by following 1:50 for input and 1:10 for the ChIP sample. Each reaction contained 0,25µl of both forward and reverse primer (final concentration: 3.1 mM), 2,5µl of template, 5µl of RealQ MasterMix, and 2µl of H_2O. qPCR reaction was set according to the manufacturer's directions with the annealing temperature of the primer at 62°C.

4.9. SDS-PAGE and Western Blot

For the preparation of protein loading on an SDS-PAGE gel, cell lysates were boiled at 95°C for 5min and centrifuged at max g for 15min. 15-20µl of sample and 2-2,5µl of protein ladder were loaded on the gel, and electrophoresis was started at 75V with constant voltage and increased up to 125V after samples were reached the resolving gel. SDS-PAGE was terminated according to the position of the protein ladder. On the other hand, IP samples were loaded on commercial precast gels with an amount of 30-40µl, and electrophoresis was performed with constant ampere starting with 5A and increased up to 30A over time. After electrophoresis, gels were transferred to a 1X transfer buffer to get rid of SDS. For transfer, gels were placed under a nitrocellulose membrane and sandwiched between sponges and Whatman filter paper using a cassette. Cassettes were placed on a wet transfer system, and the western blot was started at 100V with the duration of 3h with constant voltage. To avoid overheating, the transfer buffer was cold, an ice block was used, and the transfer was performed at +4°C. After transfer, nitrocellulose membranes were blocked for 1h at room temperature by gently shaking. Next, membranes were incubated with the primary antibody

dissolved in blocking buffer overnight at +4°C on a tube rotator or shaker. The next day, membranes were washed with TBS-T three times for 5min by gently shaking and incubated with HRP conjugated secondary for 1h at room temperature by ently shaking. After secondary antibody incubation, membranes were washed again with TBS-T three times for 5min by gently shaking and visualization was performed by dropping ECL or Sirius solutions on membranes placed on a black table and the signals were detected via the visualization system (GBox Chemi, Syngene, UK).

4.10. Immunofluorescence

To perform Immunofluorescence (IF) experiments, HEK293 cells were seeded on coverslips in a 12-well cell culture plate. As a negative control (secondary antibody control), extra cells were seeded on coverslips. The day after cell seeding, cells were washed with PBS three times for 5min. After the washing step, cells were incubated with 4% paraformaldehyde at 37°C for 15min for fixation, and then washed with PBS three times for 5min. To permeabilize cells, permeabilization buffer was given to cells and incubated for 30min at room temperature. Later, blocking buffer was given to cells and incubated for 1h at room temperature or overnight at +4°C. For primary antibody incubation, the blocking solution was removed, and the primary antibody diluted in blocking buffer, given to cells and incubated for 1h at room temperature. After that, cells were washed with PBS three times for 5min to get rid of excess antibodies, and Alexa Fluor secondary antibodies dissolved in the blocking solution were given to cells and incubated for 1h at room temperature in the dark. Later, the antibody solution was removed, cells were washed three times for 5min, and coverslips were placed on a glass slide containing DAPI mounting medium. After medium dried for a while, coverslips were sealed with nail polish, and cells were visualized by confocal microscopy (Leica TCS SP8, USA).

4.11. Duolink® Proximity Ligation Assay

Before starting Proximity Ligation Assay (PLA), HEK293 or SHSY-5Y cells were blocked as described under the section “Immunofluorescence”. After blocking cells, the

coverslip was placed on primary antibodies diluted in blocking solution, originating from different species with optimized concentrations and incubated for 1h at room temperature. As a negative control, single primary antibodies were given to the coverslip. After incubation, the coverslip was washed three times with PBS for 5min, placed on a prepared probe solution, and incubated for 1h at 37°C in a humidity chamber. Then, the coverslip was washed three times with PBS for 5min, and ligation between probes was applied using the ligation solution in the kit. It was prepared and incubated for 45 min at 37°C in a humidity chamber. At the end of PLA, the coverslip was washed three times with PBS for 5min, and an amplification reaction was carried out by placing coverslips in a polymerization solution and incubating for 120-150min at 37°C in a humidity chamber in the dark. Later, the coverslip was washed with 1X Buffer B and 0,01X Buffer B for 5 and 1min, respectively. Lastly, the coverslip was mounted with mounting medium with DAPI and sealed with nail polish on a glass slide, and cells were visualized by confocal microscopy (Leica TCS SP8, USA).

4.12. Bacterial Culture

To perform bacterial culture procedures, chemically competent cells were prepared. Firstly, 50µl of Stbl3 or DH5α–competent cell was defrosted, mixed with 5ml of LB broth and incubated at 37°C on a shaker until OD_{595} reached 0,4-0,6. After the OD_{595} value was reached in an acceptable range, the culture was centrifuged for 10min, 3000rpm at +4°C, and the supernatant was removed. Secondly, the pellet was resuspended with 12,5ml of ice-cold 50mM $CaCl_2$ and incubated on ice for 30min. Thirdly, cells were pelleted by centrifugation for 10min, 3000rpm at +4°C, and resuspended with 2,5ml of ice-cold, sterile 10% glycerol. Finally, cells were aliquoted into microfuge tubes at 50µl, flash-frozen using liquid N_2 or dry ice, and stored at -80°C for longterm use.

The transformation was performed to create competent cells carrying plasmid, which was the goal. To begin with, 5µl of plasmid was mixed with 50µl of a competent cell, incubated on ice for 30min. After incubation, the sample was incubated at 42°C for 1min and

then put on ice for 2min by moving carefully. Then, 500µl of LB Broth not containing antibody was added to the sample and incubated at 37°C for 1h on a shaker. Later, cells were centrifuged, 300µl of supernatant was removed, and the pellet was resuspended with the remaining LB broth and spread on an antibiotic-containing LB agar plate. Finally, plates were incubated overnight at 37°C. The next day, single colonies appeared on the plate. It should be noted that negative and positive controls must be included in this experiment if competent cells or plasmids are to be used every time.

Plasmid-carrying competent cells were stored at -80°C for further use. To preserve these cells, 1ml of bacterial culture in LB broth was mixed with 1ml of 50% sterile-filtered glycerol and stored at -80°C

4.13. DNA Isolation from Bacteria

To isolate DNA from competent bacteria, cells from glycerol stock at -80°C or a single colony were dropped in LB Broth and incubated overnight at 37°C on a shaker at 220rpm. After inoculation, cells were pelleted by centrifuging at max g for 10min, and the supernatant was removed. A midi-prep protocol was performed using a kit (Zymo PURE II Plasmid MidiPrep Kit, Zymo Research, USA). At the end of the protocol, the plasmid was dissolved in 500µl of autoclaved and UV-treated ddH_2O, and DNA concentration, A260/A280, and A260/A230 ratios were measured by nanodrop.

To isolate plasmid DNA without using a kit, the CTAB method was used. For 5ml bacterial culture, cells were pelleted by centrifuging at 11.000 x g for 1min, and the supernatant was removed. The pellet was resuspended in 250µl of Buffer I, and resuspension was transferred to 2ml microfuge tubes. 250µl of Buffer II was added, and the tube was gently inverted about six times and incubated for 5min by inverting gently. After incubation, 250µl of Buffer III was added to the solution, and the suspension was shaken vigorously. It should be noted that the solution appeared cloudy. To get rid of cell debris, the solution was centrifuged at 14.000rpm for 10min and replaced with ~700µl of supernatant into a new microfuge

tube. RNaseA was added to supernatant with the final concentration of 0,5ng/µl and incubated at 42°C for 20min on a shaker with 650rpm. After RNaseA treatment, 62,5µl of CTAB was added, mixed gently, and centrifuged at 14.000rpm for 10min, and the supernatant was removed. Later, 300µl of isopropanol was added to a new 1.5ml microfuge tube, the pellet was resuspended with 600µl of Buffer III, and resuspension was transferred to the isopropanol-containing tube. After that, up to 700µl of the solution was placed on a DNA binding column and centrifuged at 11.000 x g for 1min and flow-through was discarded. This step was repeated for the remaining solution. The column was washed twice with 700µl of ice-cold 70% EtOH and centrifuged at 11.000 x g for 1min, and flow-through was discarded. To get rid of the remaining EtOH, centrifugation was repeated. Lastly, the column was placed on a microfuge tube and 30-50µl of ddH_2O was added directly to the column, and incubated at 50-55°C for 5min and centrifuged at 14.000 x g for 1min.

4.14. Footprint Tests

6-week old C57BL/6 mouse was trained for the footprint test a week prior. A platform was set with 15x42mm white paper, blocks on long sides, and a dark, cave-like structure containing treat food. The front and hind paws of the mouse were colored differently with food coloring. The mouse tried to walk on the platform until it moved straight. The distances between limbs were measured and noted in Excel. Further analysis will be elaborated on in the results section.

4.15. Data Analysis and Quantification

Duolink® Proximity Ligation Assay (PLA) was quantified by selecting ≥50 cells having ≥2 dots per cell, which was considered a positive result according to two independent experiments. To test the significance, an unpaired t-test between the groups was performed. Dot plot graphs were drawn using Prism v9 Software (GraphPad, USA). Error bars represent the SEM of values.

Confocal microscopy images were processed using LAS X software (Leica, USA) or ImageJ Fiji (NIH, USA). ChIP-qPCR data were analysed by the ΔΔCT method, and each sample was normalized to corresponding input data. Significance was tested by using a t-test assuming unequal variances. Grouped column graphs were drawn using Prism 9 Software (GraphPad, USA). Error bars represent the SD of ≥3 qPCR amplicons. Analysis of the tertiary structure of Cas9 taken from PDB was performed on PyMOL v2 software (Schrodinger, USA).

5. RESULTS

5.1. Functional and Physiological Characterization of Truncated NEK1

5.1.1. Clearance of tNEK1 Aggregates by IFN Treatment

Previous studies in our lab indicated that IFN treatment caused a reduction in the number of cellular (nuclear) tNEK1 protein aggregates (Öztürk, 2015), and that tNEK1 was a PML NB client protein. To confirm and quantify the results, immunofluorescence (IF) assay was repeated. Results show a significant decrease in the number of tNEK1 aggregates upon IFN treatment (Figure 5.1). Since one of the major protein degradation processes is proteasome machinery, in order to show that clearance of aggregates upon IFN treatment is a proteasomal-dependent process, proteasome was inhibited by MG132. Under those conditions, the clearance of tNEK1 aggregates by IFN was inhibited by MG132 treatment. This situation was suggested to be caused by the depletion of proteasomal degradation of proteins. Therefore, IFN-induced clearance of tNEK1 aggregates by degradation of the protein was confirmed.

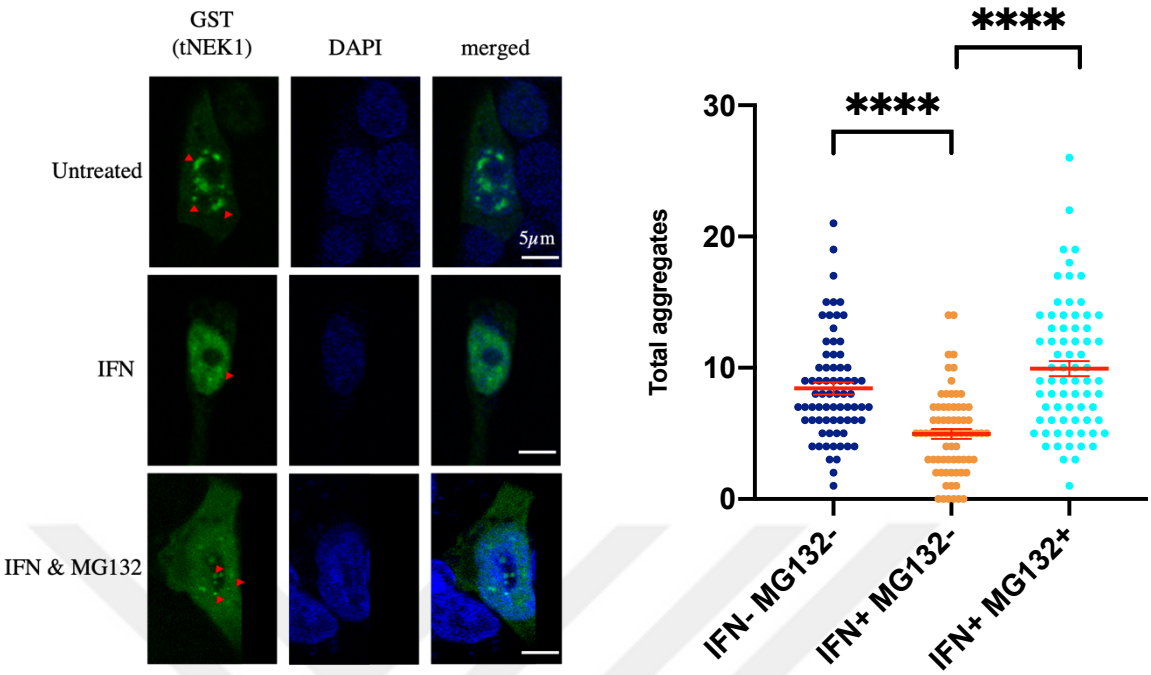

Figure 5.1. IFN treatment clears tNEK1 aggregates by protasome. Number of aggregates were decreased under IFN treatment, but the decrease was restored under both IFN and MG132 treatment. Quantifications were considered according to number of aggregates per cell. DAPI: blue, GST: green.

5.1.2. tNEK1 is Recruited to PML NBs under IFN Treatment

To confirm the recruitment of tNEK1 to PML NBs under IFN treatment, co-localization of tNEK1 and PML proteins were assessed. This was examined based on juxtaposition and overlap. IF results show that there was no co-localization of tNEK1 and PML under untreated conditions, and IFN treatment did not change this situation (Figure 5.2). Although, when cells were treated with both IFN and MG132, the overlap of tNEK1 and PML was significantly increased. To sum up, the results support the previous observations that IFN treatment leads to the recruitment of tNEK1 to PML NBs, resulting in the degradation of aggregates.

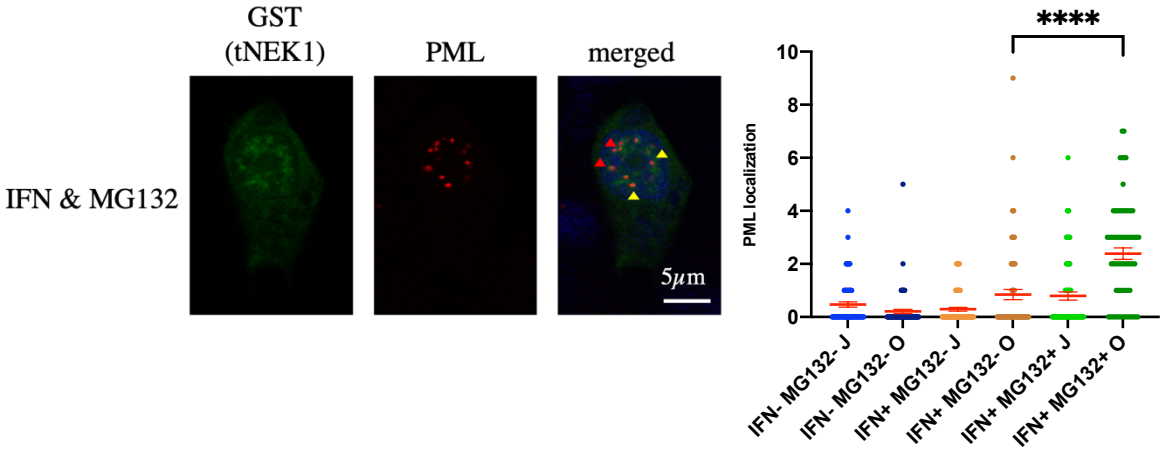

Figure 5.2. Overlap with PML was significantly increased when cells treated with both IFN and MG132 . Quantifications were considered according to localization with PML per cell. Arrowheads indicate overlap (red) and juxtaposition (yellow) of GST with PML. J: juxtaposition, O: overlap, DAPI: blue, GST: green, PML: red.

5.1.3. Effect of IFN Treatment on tNEK1 Sumoylation in Neuronal Cell Lines

Previous studies showed an increase in sumoylation of tNEK1 when HEK293 cells were treated with IFN (Öztürk, 2015). Since ALS is a neuronal disease, the experiment was repeated on neuroblast cells from neural tissue (SH-SY5Y) to investigate the presence of a similar pattern in neuronal cell lines. We performed a PLA experiment to compare the interaction between tNEK1 and SUMO proteins. No change was observed in IFN-treated SH-SY5Y cells, considering the degradation of tNEK1 facilitated by IFN (Figure 5.3). Since sumoylation is related to the degradation of proteins, we treated cells with MG132. The result showed that SUMO1 modification of tNEK1 was significantly increased under both IFN and MG132 treatment, giving a similar result to the previous experiment we performed on HEK cells. Hence, IFN treatment promotes SUMO1 modification of tNEK1, and subsequent proteasomal degradation.

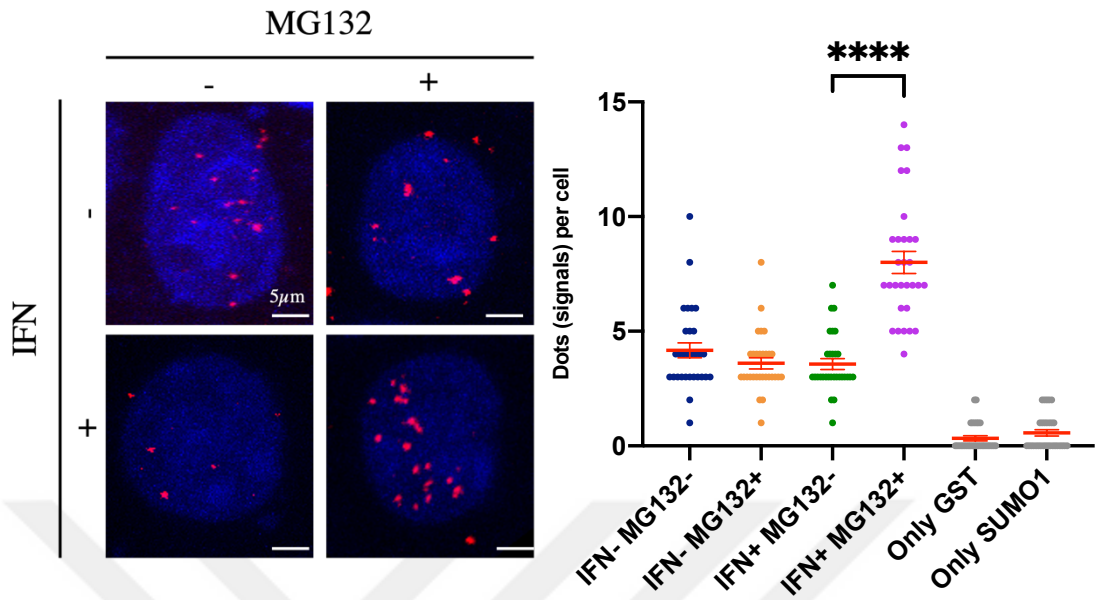

Figure 5.3. IFN treatment increases SUMO1 modification of tNEK1 in SH-SY5Y cells. While under IFN treatment tNEK1-SUMO1 interaction does not change, with the presence of IFN and MG132, the interaction significantly increases when compared to untreated condition. Since there is no significant signal counted on only primary controls, images were not shown. DAPI: blue, PLA signals: red.

5.1.4. The Effect of PML NBs on SUMO and Ubiquitin Modifications of tNEK1

Since PML NBs recruit sumoylated proteins, hypersumoylation of tNEK1 may occur in PML NB. To eludicate this hypothesis, PLA experiments were performed to analyse the change of tNEK1-SUMO interaction when PML was silenced by small interfering RNA (siPML). It was observed that there was a slight but significant decrease in tNEK1-SUMO1 interaction when PML was silenced in both HEK and SH-SY5Y cells (Figure 5.4a and c). On the contrary, no significant change was observed for tNEK1-SUMO2/3 interaction in HEK cells (Figure 5.4d). Since it was shown that tNEK1 undergoes proteasomal degradation, we investigated whether the degradation depends on the ubiquitylation of tNEK1. PLA experiments conducted to analyse tNEK1-Ubiquitin interaction showed that when PML was silenced by siRNA, the interaction was significantly decreased in SH-SY5Y cells (Figure 5.4b). As a result, hypersumoylation (for SUMO1) and ubiquitylation of tNEK1 are dependent on PML NB recruitment, but SUMO2 conjugation is not. Unfortunately, no data exists

for tNEK1-SUMO2/3 in SH-SY5Y cells and tNEK1-Ubiquitin in HEK cells. Further experiments are needed to show those interactions on relevant cell lines.

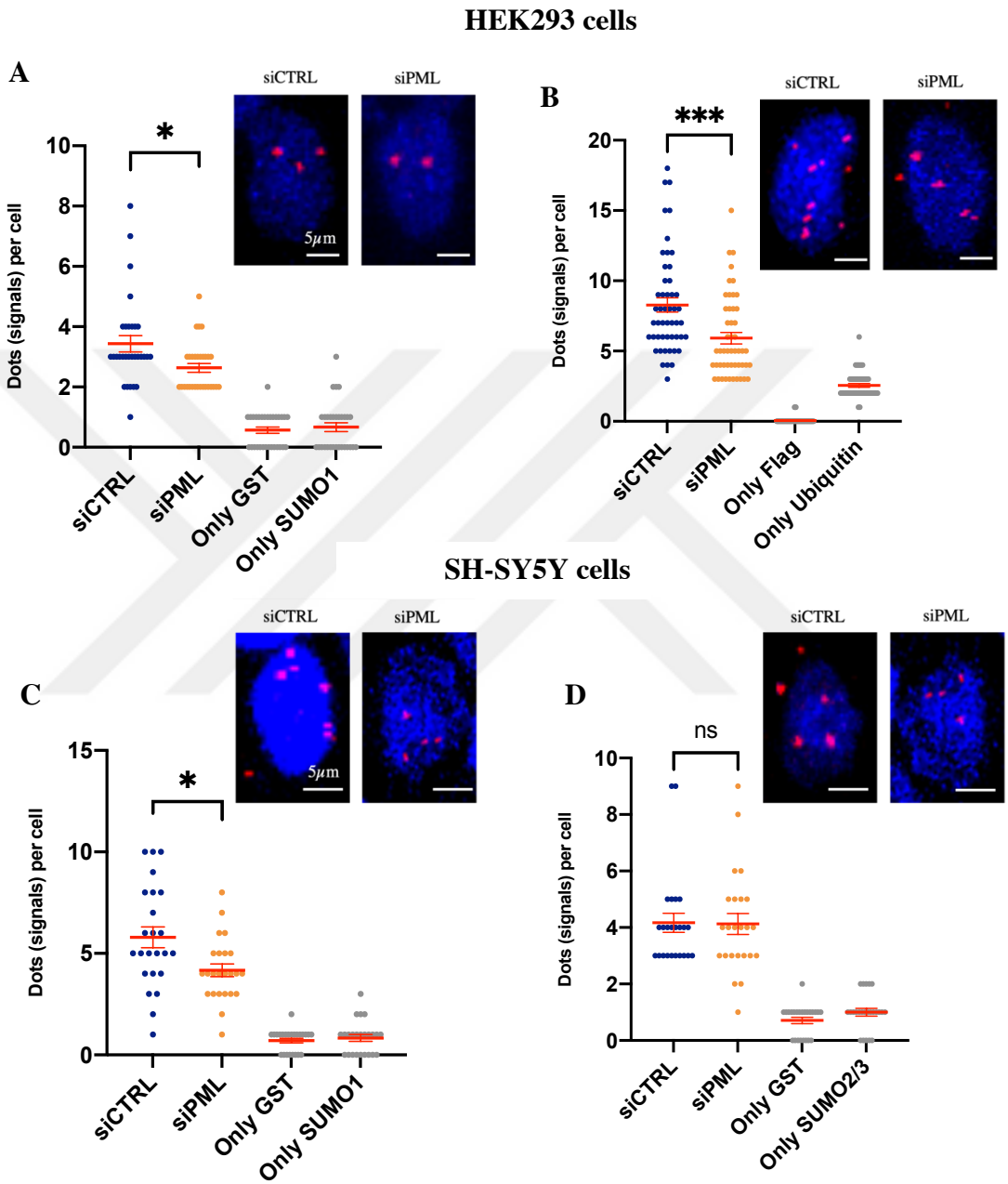

Figure 5.4. Ubiquitylation and hypersumoylation of tNEK1 occur in PML NBs. (A and B) Changes of tNEK1-SUMO1 and tNEK1-Ubiqutin interaction was shown on HEK293 cells under PML silencing by PLA. (C and D) The interaction of tNEK1 with SUMO1 and SUMO2/3 under PML knockdown were shown on SH-SY5Y cells. DAPI: blue, PLA signals: red.

5.1.5. Performing Footprint Tests for Nek1- and tNek1-expressing BALB/c Mouse

To assess motor function changes in a mouse model for ALS disease, we generated mice expressing homozygous (t/t) or heterozygous tNek1 mutations. These transgenic animals were subjected to walking and footprint assays. In addition, since tNEK1 is recruited to PML NBs and degraded according to *in vitro* studies, we also generated $pml^{-/-}$ expressing mouse with homozygous or heterozygous tNEK1 genotype. Four week old (wo) mice were trained to get used to the environment and tasks. In the sixth week, tests were begun and continued for every two weeks until the 50^{th} week. The distances between their limbs based on the parameters were measured and noted (Figure 5.5). These parameters are forelimb and hindlimb stride lengths (FS and HS), width of front and hind bases (WF and WH), and the overlap between forelimb and hindlimb (OFH). A table containing mice numbers, day of the test, ages of mice, and their footprint measurements were made. Another table containing information about mice, day of birth, and genotype was also made.

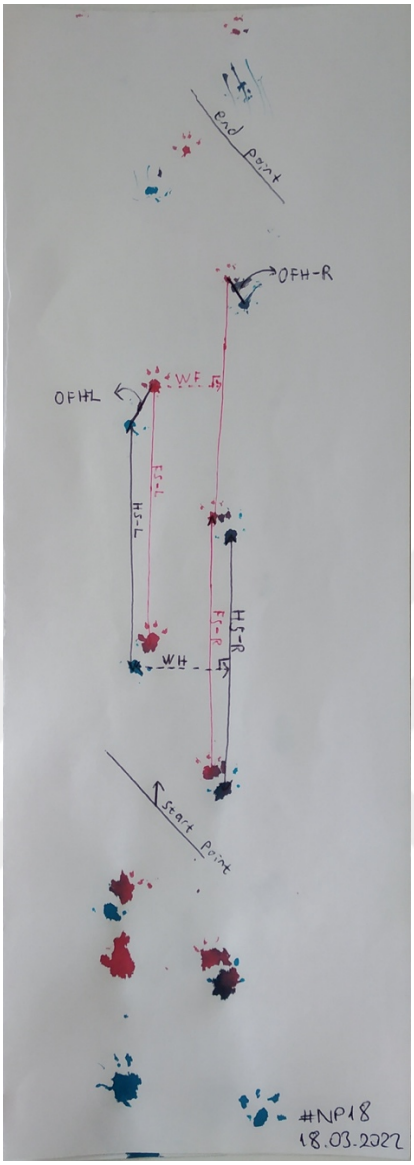

Figure 5.5. An example for footprint test. forelimb and hindlimb were coloured with red and blue, respectively. The footprint measurements were named and abbreviated as described in the text.

5.1.6. Data Processing of Footprint Measurements

To get relevant data for footprint measurements, some calculations were processed. Firstly, the mean value of multiple measurements of a mouse for each week was calculated in Excel. Secondly, the mean value of right and left measurements of FS and HS were also taken. Lastly, an absolute subtraction between FS-R and FS-L and HS-R and HS-L were made to calculate the asymmetry of walking (As-R and As-L). After processing the data,

line graphs were made for each analysis according to the age of an animal. For all genotypes, error bars were made for each week by considering SEM. It should also be noted that no mice expressing t/t and t/t $pml^{-/-}$ were left after 38^{th} and 32^{nd} weeks, respectively, because they got sick and died.

5.1.7. Normalization of Footprint Data

As a phenotypical outcome, the length of a mouse with a t/t genotype is smaller than a wildtype mouse, so it may also affect stride. So, all data on stride length and width base were divided into the average length for the same genotype. It should be considered that, since data for the length of mice were taken at later stages of the experiment, we must use the average length by considering the age and genotype of the mice. After normalization to length, there were no apparent differences among subjects (Figure A.1). Although, it should be noted that there is a weekly decreasing trend in mice having t/t, t/t $PML^{-/-}$, and heterozygous $PML^{-/-}$ genotypes.

To more easily see a decreasing trend, all measurements were divided into the first week's measurements corresponding to genotype, which results in starting at the same level. To make lines smoother, a LOWESS approach was also taken. Based on these graphs, there is a significant decrease in width bases in mice having t/t and t/t $PML^{-/-}$ genotypes (Figure 5.6). However, contrary to our expectations, there is no difference between t/t and t/t $PML^{-/-}$ on any of the measurements. We should expect a worsening phenotype in the absence of PML; like in our hypothesis, PML prevents the aggregation of tNEK1 by promoting proteasomal degradation.

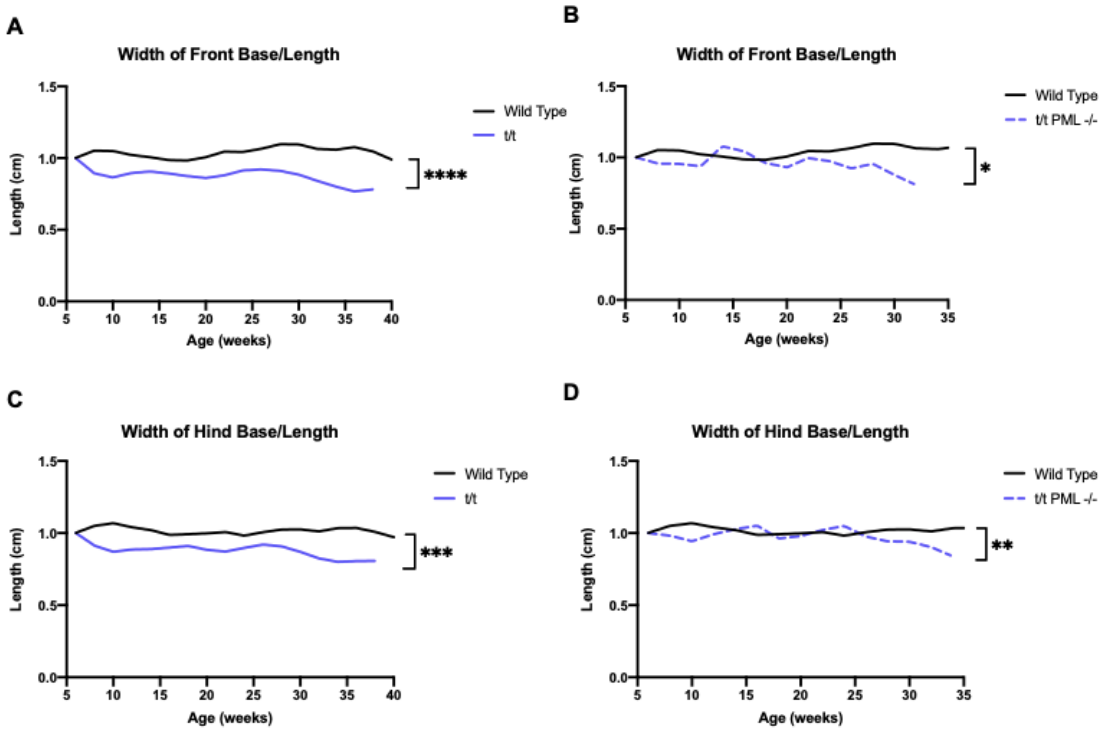

Figure 5.6. Footprint analysis of mice.

5.2. Discovery of Cas9 Sumoylation Site and Its Consequences on Cas9

5.2.1. In silico Analysis of Cas9 Sumoylation Predicted Sites

Our previous lab members showed that *S. pyogenes* Cas9 has 10 sumoylation consensus motifs (ψKxD/E) (Yeşildağ, 2019). Figure 5.7 shows the lysine residues on primary and tertiary structures of Cas9. According to the tertiary structure, nine SUMO motifs are located on the protein's surface, and the remaining one (K1148) is located inside the protein, excluding the possibility of a sumoylation site.

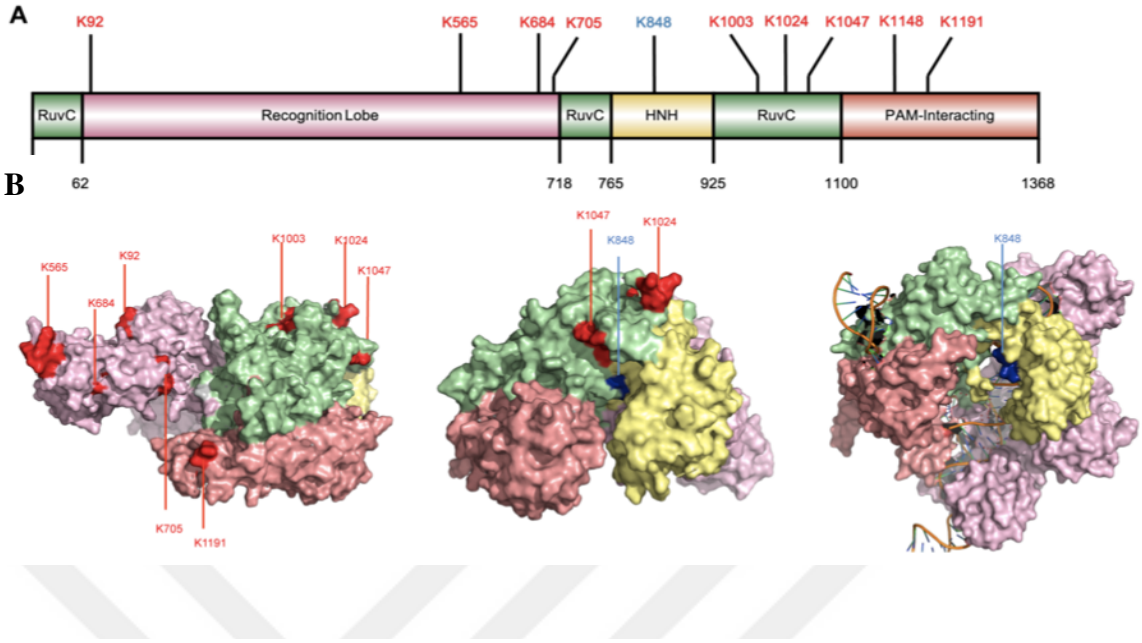

Figure 5.7. Structure of Cas9. Domains and SUMO motifs of Cas9 are shown in secondary (A) and tertiary (B) structures. Sumoylation site of Cas9 were indicated as blue. Conformational change and exposure of the K848 site when Cas9 bind to DNA should also be considered (B, on the right). The data were taken from Protein Data Bank. Left and middle (pdb: 4CMP) and right (pdb: 4OO8).

5.2.2. Endogenous Sumoylation of Cas9

To investigate whether Cas9 is endogenously sumoylated, HEK293 cells were transfected with pCW-Cas9 for an IP assay. FLAG-tagged Cas9 was pulled-down by anti-FLAG antibody, and sumoylated proteins were visualized by SUMO1 and SUMO2/3 blots. Results show that Cas9 is endogenously sumoylated by SUMO1 and SUMO2/3 (Figure 5.8a and b). To support this result, Proximity Ligation Assay (PLA) was performed. In this experimental setup, the interactions of Cas9 with SUMO1, SUMO2/3 and UBC9 were investigated under endogenous expression of SUMO1, SUMO2/3, and UBC9 in Cas9-stable HEK cells (Figure 5.8c). As negative controls, primary antibodies were used separately. When negative controls were considered, results proved the theory of Cas9 sumoylation and interaction with UBC9, which is an obligate enzyme for sumoylation.

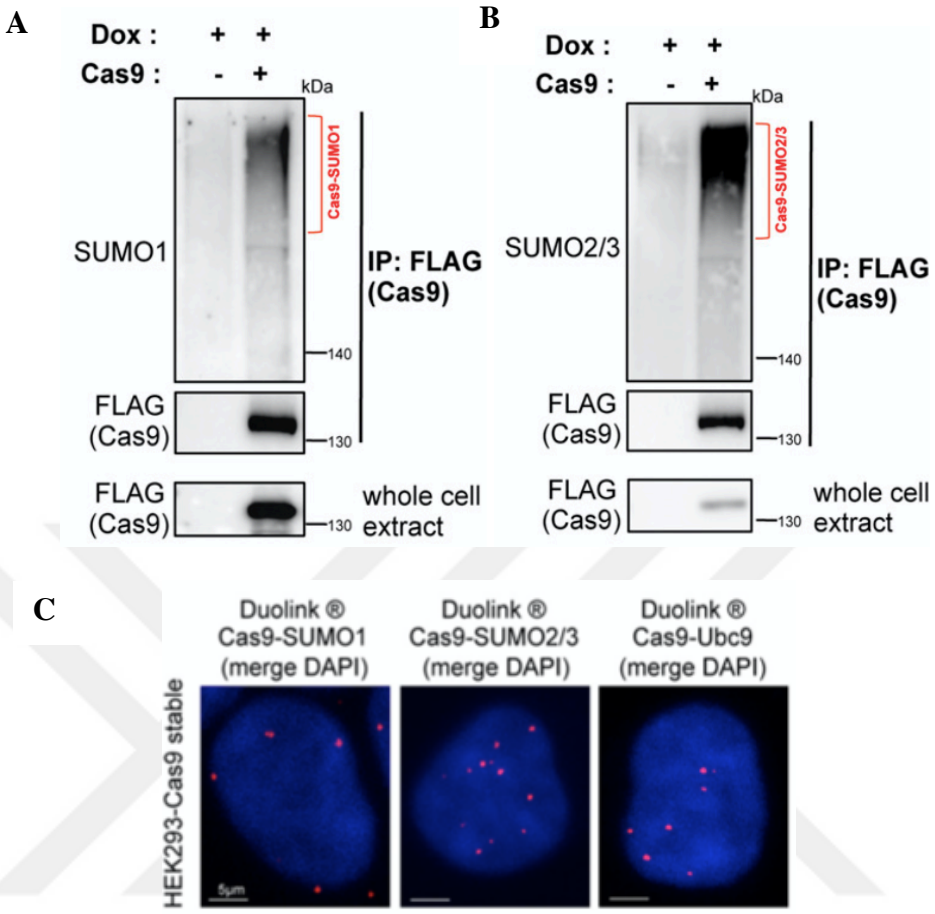

Figure 5.8. Cas9 sumoylation occurs in endogenous systems. SUMO1, SUMO2/3 and UBC9 interactions with Cas9 was shown by performing IP (A and B) and (C) PLA experiments. Since there is no signal in single primary antibody controls, they were not shown. DAPI: blue, PLA signal: red. PLA assay was performed in collaboration with Özgecan Ayhan.

5.2.3. Determining Cas9 Sumoylation Site(s)

After *in silico* analysis of Cas9 sumoylation motifs, IP experiments identified the sumoylation site(s) of Cas9. Previously, each of ten lysine residues of SUMO motifs on Cas9 was mutated to arginine amino acid in order to impair sumoylation of the protein. HEK293 cells were transfected with wildtype, mutated versions of FLAG-tagged Cas9, and either SUMO1 or SUMO2. FLAG-tagged proteins were pulled-down by FLAG antibody with resin beads and immunoblotted with SUMO1 or SUMO2/3 antibodies. None of the mutants

showed any significant sumoylation deficiency in SUMO1 overexpressed groups, while one of the mutants ($Cas9^{K848R}$) showed a significant decrease in sumoylation of Cas9 in SUMO2 overexpressed groups when compared with $Cas9^{WT}$ (Figure 5.9). Thus, we concluded that K848 is the major SUMO2 conjugation site; however, we could not find the SUMO1 conjugation site.

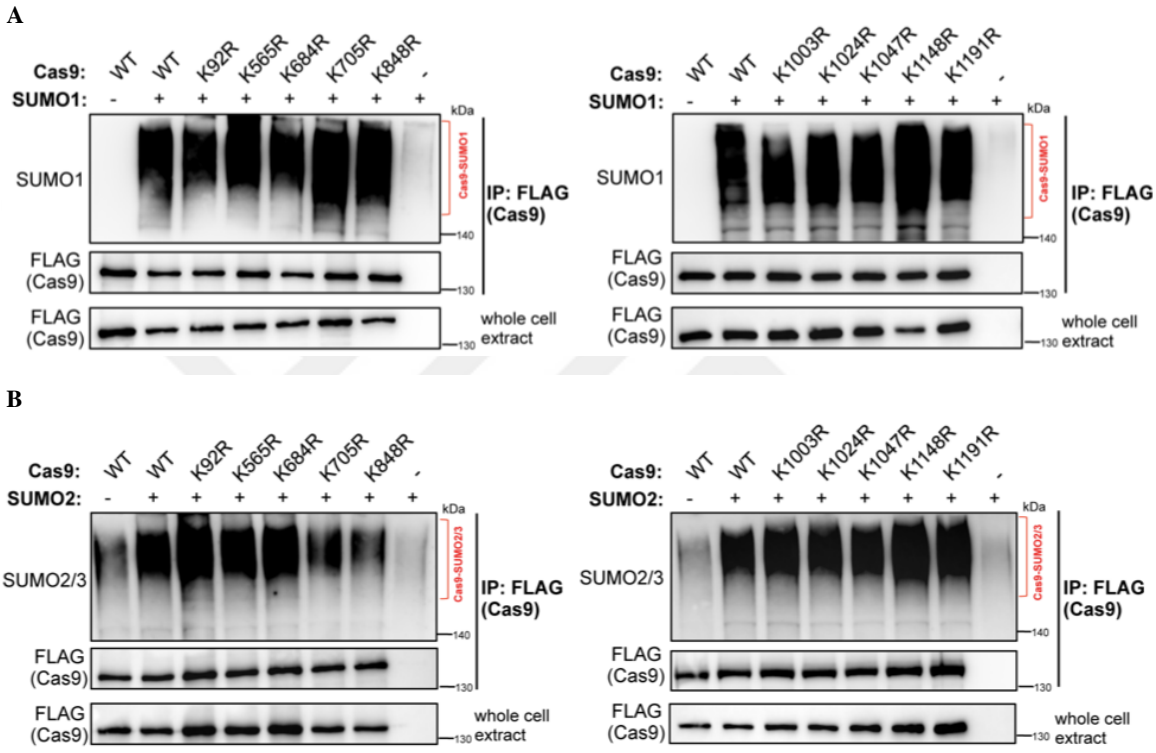

Figure 5.9. Determination of SUMOylation site(s) on Cas9 protein. IP experiments with 10 SUMO motif deficient mutants were performed under Cas9 and SUMO1 (A) or SUMO2 (B) overexpression conditions.

5.2.4. Confirmation of K848 as The Major SUMO2/3 Conjugation Site for Cas9

To ensure that K848 is the major sumoylation site for Cas9, IP was performed on $Cas9^{WT}$ and $Cas9^{K848R}$ transfected HEK293 cells under both SUMO overexpression and endogenous expression conditions. Under both conditions, FLAG-tagged Cas9 samples were pulled-down and immunoblotted with SUMO2/3 antibody. As a result, a deficiency in $Cas9^{K848R}$ sumoylation was observed when compared with the $Cas9^{WT}$ sumoylation under both over-expression and endogenous sumoylation conditions (Figure 5.10a and b). To

analyze the SUMO1 modification of Cas9, IP and PLA assays were performed under endogenous SUMO expression; however, there was still no notable decrease in SUMO1 conjugation level of Cas9^{K848R} observed (Figure 5.10c and d). These results confirm that K848 on Cas9 is the major conjugation site for SUMO2/3, but not for SUMO1.

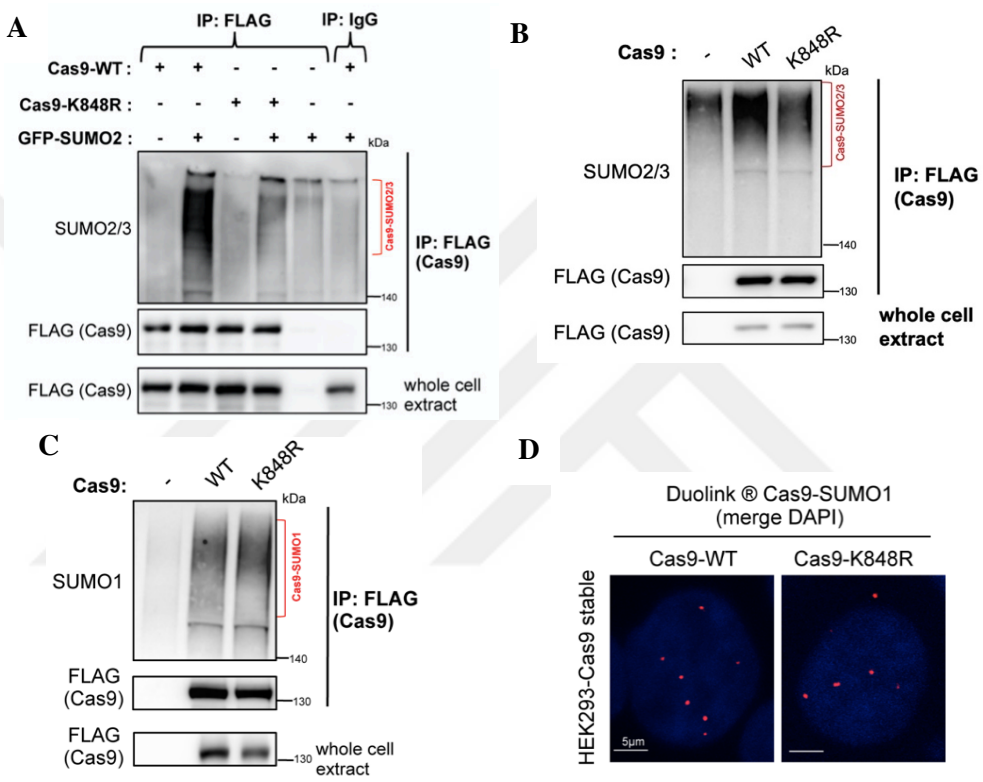

Figure 5.10. SUMO2/3 conjugation of Cas9 on K848 residue. IP assay was performed with wild type and mutant Cas9 under both overexpression (A) and endogenous expression (B) of SUMO2/3. (C and D) SUMO1 conjugation of Cas9^{K848R} analyzed by both IP (C) and PLA assays (D). Since there is no signal in single primary antibody controls, they were not shown. DAPI: blue, PLA signal: red. PLA assay was performed in collaboration with Özgecan Ayhan.

5.2.5. Investigation of Cas9^{D850A} Sumoylation

It is possible that sumoylation deficiency of Cas9^{K848R} may not depend on the mutation from lysine to arginine. It can also be caused by other conditions such as changes in the

tertiary structure of the protein, like misfolding. To learn what causes sumoylation deficiency, aspartic acid (D850) which resides next to the lysine (K848) residue in the SUMO motif (LKDD) was mutated to alanine, $Cas9^{D850A}$, which is supposed to deplete sumoylation since SUMO motif is destroyed. IP experiments were performed on $Cas9^{WT}$, $Cas9^{K848R}$ and $Cas9^{D850A}$ samples by pulling-down the FLAG-tagged Cas9 and immunoblotting by SUMO2/3 antibody. At first, the experiment was performed by overexpressing SUMO2; however, the decrease of sumoylation in the $Cas9^{D850A}$ mutant was not observed (not shown). Since this may be caused by unnatural overexpression conditions, which is possible to result in unspecific SUMO modification of the protein, the experiment was repeated under endogenous sumoylation conditions, which is more reliable than overexpression. The result shows a significant deficiency in sumoylation of $Cas9^{D850A}$, similar to $Cas9^{K848R}$ when SUMO levels were compared with $Cas9^{WT}$ (Figure 5.11a).

To support the IP results, PLA was performed on the $Cas9^{D850A}$ mutant under endogenous expression conditions. PLA results also showed a significant decrease in Cas9-SUMO2/3 interaction for the $Cas9^{D850A}$ mutant, like in the case for $Cas9^{K848R}$, when signals belonging to $Cas9^{WT}$ were compared (Figure 5.11b). Therefore, both PLA and IP results under endogenous expression conditions confirm that K848 is the major sumoylation site, and sumoylation deficiency is unrelated to the change in the protein's tertiary structure.

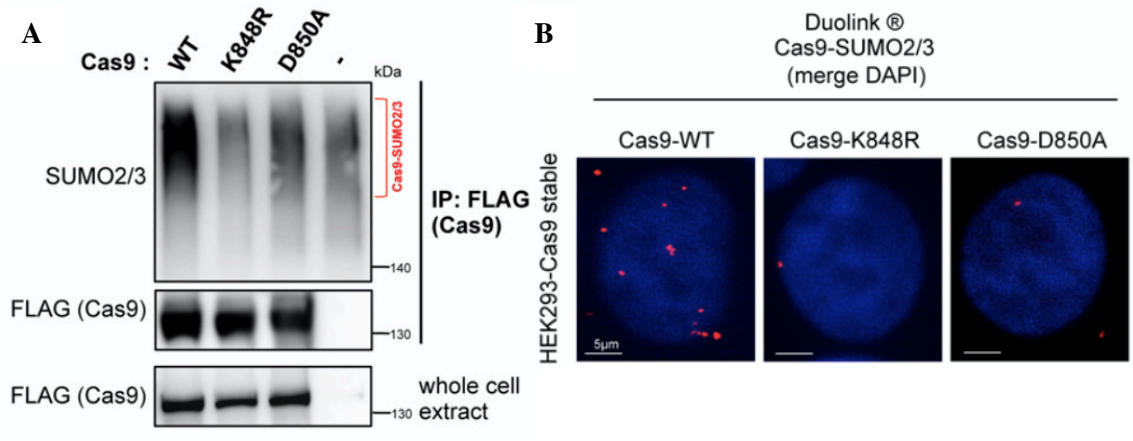

Figure 5.11. D850A mutation proves the sumoylation deprivation in Cas9. Sumoylation deficiency of Cas9^{D850A} mutant was shown by IP (A) and PLA (B) assays in HEK293 cells when SUMO is expressed endogenously. Since there is no signal in single primary antibody controls, they were not shown. DAPI: blue, PLA signal: red. PLA assay was performed in collaboration with Özgecan Ayhan.

5.2.6. Ubiquitylation of Cas9

According to previous experiments performed by A. B. Celen, Cas9 is also ubiquitylated (Celen, 2019). Because assays were performed with overexpression of Ubiquitin, this may give misleading results. To reinforce the results, the experiment was repeated under endogenous expression conditions. Since ubiquitylation is related to the degradation of proteins, some samples were treated with proteasome inhibitor MG132. IP and PLA assays show that Cas9 is ubiquitylated and then undergoes degradation (Figure 5.12). This result indicates that the degradation of Cas9 is a Ubiquitin-dependent process.

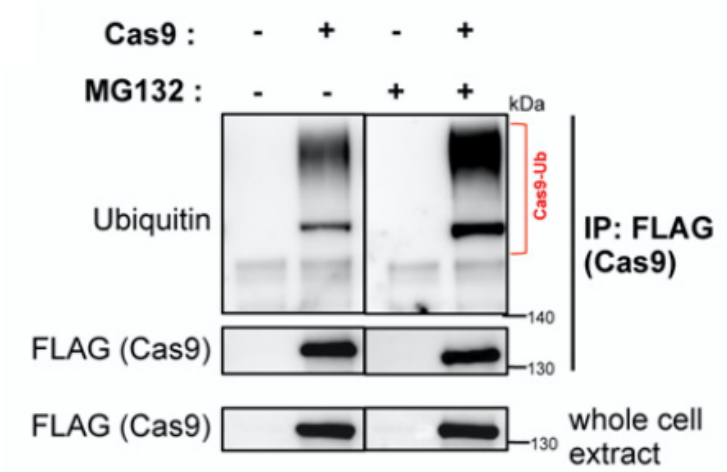

Figure 5.12. Cas9 is ubiquitylated and then degraded by proteasome. (A) Under endogenous conditions, ubiquitylation of Cas9 was shown by IP assay.

5.2.7. Sumoylation Prevents Cas9 from Being Ubiquitylated

According to mass spectrometry assay results performed by a previous lab member, Cas9 has 14 ubiquitylation sites (Celen, 2019). Interestingly, K848 was also one of them. So we investigated Cas9 ubiquitylation on a SUMO deficient mutant by performing IP and PLA assays. Since the ubiquitylation of proteins mostly undergoes proteasomal degradation, samples were also treated with a proteasome inhibitor, MG132. IP with FLAG-tagged Cas9 and His immunoblot shows that the ubiquitylation of Cas9 is significantly increased with K848R mutation under MG132 treatment (Figure 5.13a). In addition, PLA was also confirmed for the significant increase in ubiquitylation of $Cas9^{K848R}$ mutant under MG132 treatment (Figure 5.13b). These findings show that sumoylation interferes with ubiquitylation of Cas9 and may affect the stability of the protein by preventing Ubiquitin-dependent proteasomal degradation.

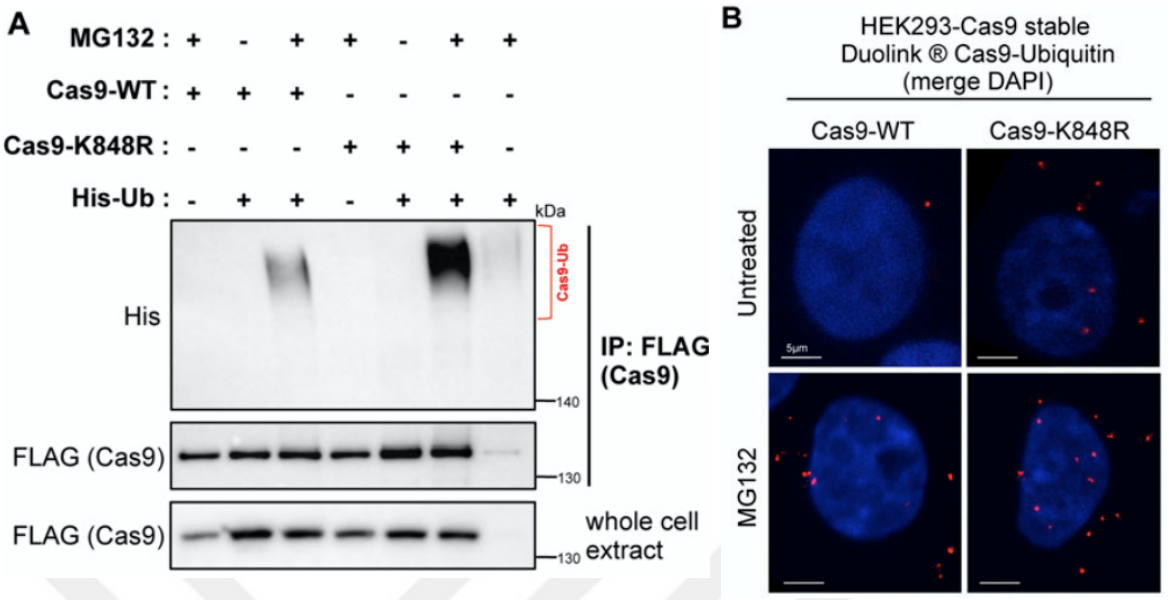

Figure 5.13. Sumoylation deficiency inreases ubiquitylation of Cas9 which leads to degradation. Ubiquination of $Cas9^{WT}$ and $Cas9^{K848R}$ was assased by IP (A) and PLA (B). Since there is no signal in single primary antibody controls, they were not shown. (DAPI: blue, PLA signal: red). PLA assay was performed in collaboration with Özgecan Ayhan.

5.2.8. Subcellular Localization of Cas9 SUMO Deficient Mutants

We realized from previous PLA experiments that, while sumoylated Cas9 localized in the nucleus, ubiquitylated Cas9 appeared in the cytoplasm (Figure 5.11b and Figure 5.13b). So we investigated the impact of SUMO conjugation on Cas9 subcellular localization. To that end, the localization of SUMO deficient Cas9 mutants was compared by IF. As for wildtype Cas9, the localization of $Cas9^{K848R}$ and $Cas9^{D850A}$ was both cytoplasmic and nuclear (Figure 5.14). These results show that sumoylation does not affect the subcellular localization of Cas9.

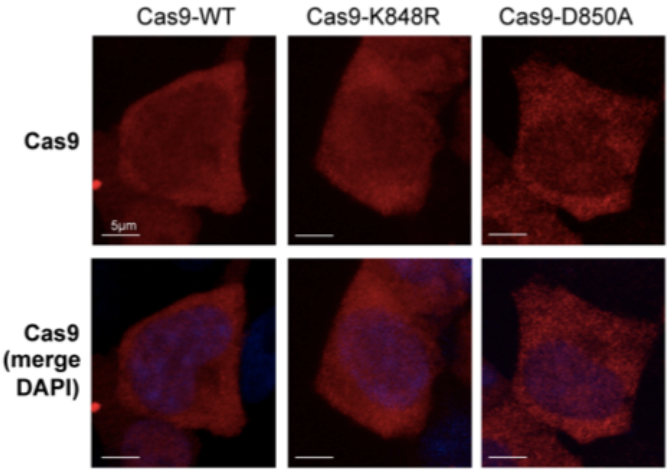

Figure 5.14. Localization of Cas9. Wildtype and SUMO deficient mutant Cas9 proteins were shown in both cytoplasmic and nuclear part of the cell. DAPI: blue, Cas9: red.

5.2.9. Impact of Cas9 Sumoylation on DNA Binding Ability

Since K848 is located on a critical site at the Cas9's HNH endonuclease domain, sumoylation may affect its DNA binding ability. To test this hypothesis, ChIP experiments were performed to compare the DNA binding efficiency of wildtype and sumoylation-deficient Cas9. In the experimental setup, sumoylation of Cas9 was depleted in two ways; by using Cas9 SUMO-deficient mutants ($Cas9^{K848R}$ and $Cas9^{D850A}$) or inhibiting global sumoylation with ML792, a drug that blocks SUMO E1-activating enzyme, and gRNAs were used to target the promoter region of pS2 (TFF1), and Interferon Regulatory Factor 4 (IRF4). Before performing ChIP, catalytically dead versions of Cas9 ($dCas9^{K848R}$ and $dCas9^{D850A}$) were made by Özgecan Ayhan. It is important to mention that $dCas9^{D850A}$ is a crucial control for this experiment to discover whether the effect of DNA binding comes from a mutation of K848 as a critical acidic residue, or sumoylation deficiency. After ChIP assays, qPCR was performed to analyse the abundance of DNA in ChIP samples relative to input DNA. Considering negative controls which are nonspecific antibody (IgG) and empty gRNA (EV), in both gRNA targets, a significant decrease in fold enrichment was observed in all SUMO-deficient conditions ($dCas9^{K848R}$, $dCas9^{D850A}$ and ML792 treated Cas9) when compared to $Cas9^{WT}$ (Figure 5.15). Therefore we can conclude that sumoylation of Cas9 increases DNA binding ability.

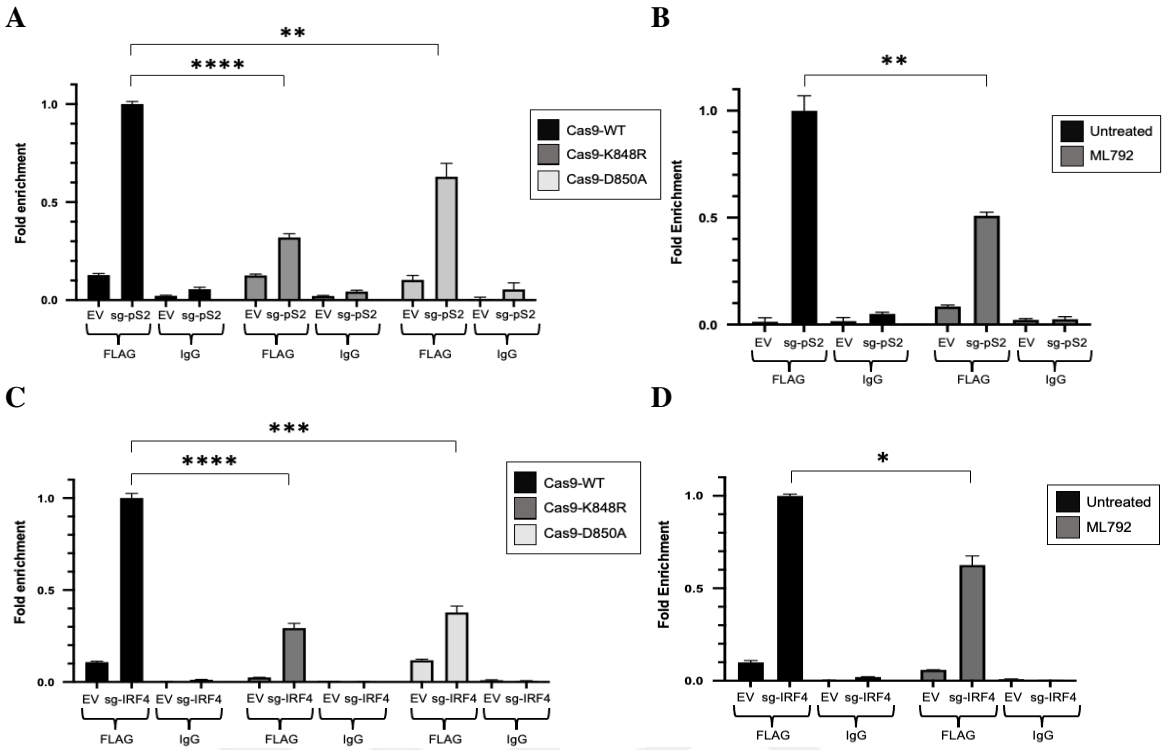

Figure 5.15. Impact of Cas9 sumoylation on target DNA binding. Sumoylation deficiency was made by using SUMO defective mutants, dCas9^{K848R} and dCas9^{D850A}, or inhibiting global sumoylation by ML792 treatment. Flag-dCas9 was pulled-down by Flag coated magnetic beads, and DNA binding ability was assessed by performing qPCR on targets ERE3 (pS2) (A and B) and IRF4 (C and D).

6. DISCUSSION

6.1. tNEK1 Aggregation, Clearance by IFN and Effects on Mouse Behaviour

Previous studies performed by our other lab members have identified the NEK1 sumoylation sites and hypersumoylation of tNEK1 (Öztürk, 2015). Besides, nuclear trap and aggregate formation were observed as characteristics of tNEK1. As sumoylated proteins localize in PML NBs, tNEK1 was also observed in those membraneless organelles when PML nucleation was induced by arsenic or IFN. Furthermore, clearance of tNEK1 aggregates was observed upon IFN treatment on cells. We also found that this process is PML-dependent and this implies that hypersumoylated tNEK1 in PML NBs undergoes Ubiquitin-dependent proteasomal degradation. Although some data show that ubiquitylation of tNEK1 is PML-dependent, results should be confirmed by other assays such as IP.

Another finding is that SUMO1-dependent hypersumoylation of tNEK1 is also a PML-dependent process; however, that is not the case for SUMO2/3. Considering the structure differences between SUMO1 and SUMO2/3, their modification rate, lysine residue, and effects on target proteins may differ as well (Matic *et al*., 2008). For instance, SUMO2/3 conjugation of Cas9 is more favourable than SUMO1 (Ergünay *et al*., 2022). Another example can be given to sumoylation of PER2, a protein involved in circadian rhythm (L.-C. Chen *et al*., 2021). On the one hand, SUMO1 modification of PER2 is suggested to contribute to S662 phosphorylation and causes transcriptional repression. On the one hand, SUMO1 modification of PER2 is suggested to contribute to S662 phosphorylation and causes transcriptional repression. On the other hand, SUMO2 conjugation leads to the degradation of the protein. Therefore, hypersumoylation of tNEK1 may be occurred by SUMO1 conjugation, which leads to Ubiquitin-dependent degradation.

Mouse behaviour tests provide information about physiological/behavioural effects of tNEK1 pathogenesis in mouse models. In addition to the footprint tests, hanging wire, rotarod, grip strength and mobility tests were performed weekly by another lab member, P.

Georgidou. Footprint tests aim to observe walking disorders like asymmetric walking, shorter steps, and broader or narrower steps. An important variable affecting some of these tests is the length of mice. It was observed that a mouse with a t/t genotype of the same age and sex is much shorter than a wildtype mouse. The measurements taken from footprint tests were divided by the average length of mice for that week, for normalization. However, the results were not significant, because no apparent effects of tNEK1 were observed. When the baseline correction was calculated by taking into account the first week's test, some of the results, namely width of front and hind bases, provided relevant output, implying that there are some walking disorders manifested in t/t mice. The proper interpretation and understanding of these results is of utmost importance in order for the consequences of tNEK1 on a mouse model to be determined, as they will alter the conditions for the proper observation of a potential recovery upon IFN treatment.

Similarly to footprint tests, the other behaviour tests had significant results. The effect of tNEK1 was more obvious when performing different tests such as rotarod, hanging wire and grip strength. For instance, in the hanging wire test performed by Panagiota; mice belonging to t/t group were moving significantly less compared to their wildtype counterpart mice. This behaviour may indicate a motility disability, becoming more noticeable under challenging conditions. In addition to their small body size, t/t mice get sick and die remarkably earlier that wildtype mice. They also suffer from polycystic kidney disease.

According to *in vitro* studies, the clearance of tNEK1 aggregates was achieved via IFN-induced PML bodies' enhancement, which led to hypersumoylation of tNEK. Because of their significance and PML-dependent clearance needing to be verified, $PML^{-/-}$ tNEK1 genotype mice were generated and included in the tests. According to our hypothesis, we predicted worsening mobility conditions for mice expressing this genotype due to increased protein aggregation. Some preliminary findings from other behavioral tests gave supportive results for this hypothesis, showing a deteriorated performance in motility and grip strength tests of the t/t $PML^{-/-}$ mouse in comparison to the t/t mouse. Unfortunately, no significant changes were observed in the t/t $PML^{-/-}$ mouse for footprint tests compared with the t/t mouse. Consequently, more tests that lend support to PML-related effects of tNEK1 on mouse models are required.

Another primary aim of performing behavioral tests is to discover the therapeutic effects of IFN treatment on mouse models. *In vitro* studies showed that IFN treatment causes PML recruitment of tNEK1, leading to SUMO1 and Ubiquitin conjugation and followed by the clearance of tNEK1 aggregates by proteasomal degradation. If the treatment also works on mouse models carrying tNEK1, a recovery phenotype for treated animals is expected. Results carry cruciality for clinical trials.

In future studies, some details need to be clarified. For example, whether tNEK1 hypersumoylation is a naturally occurring event needs to be investigated. This can be tested by tNEK1-stable cells or neuronal cells isolated from a tNEK1-expressing mouse. Also it is crucial to know whether the clearance of tNEK1 aggregates from cells by IFN treatment is related to PML nucleation; because this can play a PML-independent role. IP and PLA should be performed to observe tNEK1 ubiquitylation under PML-silenced or IFN-treated conditions. More importantly, clearance of tNEK1 aggregates from IFN-treated mouse with tNEK1 genotype should be investigated by performing cytological and histological studies. Thus, current results from both *in vivo* and *in vitro* studies have promising results for therapeutic effects of IFN treatment in NEK1-related ALS disease; however, more areas should be elucidated in pre-clinical trials.

6.2. Discovery of Cas9 Sumoylation Site and Its Effects on the Protein

In this project, the discovery of Cas9 sumoylation was enabled by determining the sumoylation site. Sumoylation of K848 residue on Cas9 was found as a major SUMO2/3 conjugation site according to IP and PLA assays, under both SUMO2 overexpression and endogenous expression. According to IP experiments, there were no other SUMO2/3 conjugation sites found for Cas9. Contrary to indications of SUMO1 conjugation under both endogenous and overexpression conditions, no SUMO1 conjugation site, including K848, was found. It should be noted that those sumoylation motifs are the only common ones in the literature; however, alternative sumoylation motifs were also found in the literature (Josa-Prado *et al*., 2015; Ulman *et al*., 2021). Possibly, SUMO1 modification on Cas9 occurs in those alternative sumoylation sites. Another possible explanation is that IP experiments with

10 sumoylation sites carrying mutations under overexpression conditions might have masked the endogenous SUMO1 deficiency. Besides, it should be considered that when sumoylation rates were compared in PLA and His pull-down assays, SUMO2/3 modification was much higher than SUMO1 modification. According to the literature, SUMO chains are often formed by SUMO2/3; however, SUMO1 stays as monomers (Liebelt and Vertegaal, 2016). So, SUMO1 modification may occur in those canonical and noncanonical SUMO motifs. To further clarify this, IP experiments under endogenous expression of SUMO1 should be performed, or non-canonical SUMO motifs need to be considered as well.

In addition to the discovery of Cas9 sumoylation, ubiquitylation of Cas9 was also identified by our previous lab member (Celen, 2019). We also proved ubiquitylation of Cas9 under endogenous expression. Moreover, it was found that ubiquitylated Cas9 undergoes proteasomal degradation. The Ubiquitin-proteasome interaction was also shown by a PLA experiment performed by Özgecan Ayhan (Ergünay *et al*., 2022). According to MS/MS study, K848 was also found to be one of the ubiquitylation sites among the 14 sites. However, we observed a significant increase in ubiquitylation of $Cas9^{K848R}$. The existence of 13 more ubiquitylation sites in Cas9 may mask the lack of deficiency. A possible crosstalk between SUMO and Ubiquitin modification of proteins should also be considered: they can act antagonistically towards or sequentially with one another, or recruit each other (Figure 6.1, Liebelt & Vertegaal, 2016). For example, USP7, an SDUB protein, functions as deubiquitylation of SUMO and sumoylated proteins, such as replisomes (Lecona *et al*., 2016). Based on this knowledge, it can be speculated that sumoylation may affect ubiquitylation of Cas9. Besides, we observed a significant decrease in protein turnover rate for sumoylation-deficient mutants and a recovery of protein stability. This finding supports the sumoylation-dependent inhibition of Cas9 ubiquitylation.

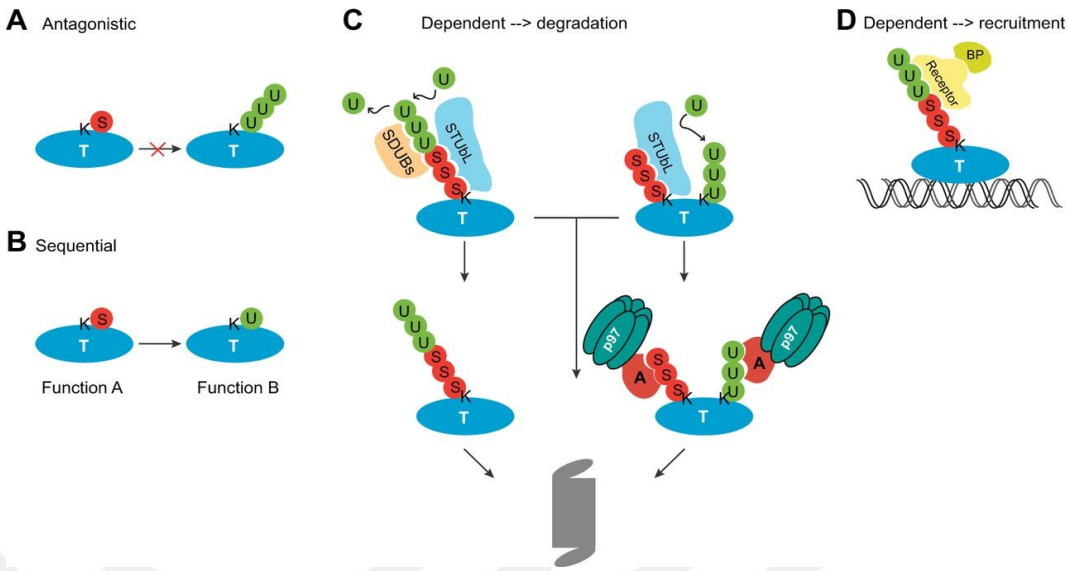

Figure 6.1. Interplay between SUMO and Ubiquitin modifications (Liebelt and Vertegaal, 2016).

Based on results of the PLA performed in collaboration with Özgecan Ayhan, sumoylated Cas9 mainly localized in the nucleus, while ubiquitylated Cas9 is enriched in the cytoplasm. This result also shows the competition or antagonism between SUMO and Ubiquitin modification of Cas9. There are two possible ways which would affect and change the localization preference of Cas9. According to the first scenario, some naked Cas9 proteins are imported to the nucleus via NLS, where also sumoylation takes place. The remaining Cas9 proteins in the cytoplasm are degraded after ubiquitylation. The other scenario is that sumoylation occurs in the cytoplasm promoting nuclear import, and ubiquitylated Cas9 stays in the cytoplasm, which leads to proteasomal degradation of the protein. The differences between these two plausible options are related to the relevance of Cas9 localization via SUMO. It should also be considered that no appearent change in localization of Cas9 on SUMO-deficient mutants was observed when compared with wildtype Cas9. Consequently, the second option seems to be the most prevalent, since a change in localization of SUMO-deficient Cas9 towards cytoplasm is expected, if sumoylation promotes the nuclear import of the protein. Therefore, we may consider that sumoylation of Cas9 occurs in the nucleus. However, the interplay between the sumoylation and ubiquitylation of Cas9 should be investigated for further elucidation of the subject.

In the literature, some studies try to increase the on-target and decrease the off-target activity of Cas9 for CRISPR. For example, Slaymaker *et al*. generated some enhanced Cas9 (eCas9), which has reduced off-target, and improved on-target activities by mutating some critical amino acids in HNH and RuvC endonuclease domains. Incidentally, K848 was also studied as one of the residues mutated to alanine amino acid. It was shown that the K848A mutation caused a significant reduction of the off-target and a slight decrease in on-target activity. Besides, in combination with other mutants (K1003A and K1060A), it boosted the reduction of off-target and enriched the on-target activities (Slaymaker *et al*., 2016). Based on this study, SUMO modification of Cas9 on K848 residue may affect the Cas9 activity. ChIP experiments showed that when Cas9 sumoylation was deprived by K848R and D850A mutations, or global sumoylation was inhibited with ML792 treatment, DNA binding on two different targets was significantly decreased. It is also essential that the presence of $Cas9^{D850A}$ in the experiment proved to have a similar pattern to $Cas9^{K848R}$ and ML792-treated samples, because this eliminates the possibility of K848R mutation affecting the DNA binding independently to sumoylation. Thus, sumoylation of Cas9 on K848 residue increases DNA binding, which produces a similar result to Slaymaker's study shown by $Cas9^{K848A}$ mutant. It is suggested that sumoylation at K848 residue makes the DNA binding site more accessible to DNA by changing the conformation of Cas9. However, more research needs to be performed to clarify the impact of Cas9 sumoylation on off-target activity and functional outcomes, and the changes in the 3D structure of Cas9 when is sumoylated.

For further studies, it is crucial for the functional consequences of Cas9 sumoylation on CRISPR activity to be investigated. This may illustrate the importance of SUMO and provide improvements for the CRISPR/Cas9 system.

To summarize, SUMO plays crucial roles in biological mechanisms, from bacteria to eukaryotes, in health and disease conditions. It has a high potential to be involved in targeted therapy, biotechnological studies, and synthetic biology in the near future.

REFERENCES

Bonafede, R. and R. Mariotti, 2017, "ALS Pathogenesis and Therapeutic Approaches: The Role of Mesenchymal Stem Cells and Extracellular Vesicles", *Frontiers in Cellular Neuroscience*, Vol. 11, No. 80, pp. 1-16.

Brenner, D., K. Müller, T. Wieland, P. Weydt, S. Böhm, D. Lulé, A. Hübers, C. Neuwirth, M. Weber, G. Borck, M. Wahlqvist, K.M. Danzer, A.E. Volk, T. Meitinger, T.M. Strom, M. Otto, J. Kassubek, A. C. Ludolph, P.M. Andersen and J.H. Weishaupt, 2016, "NEK1 Mutations in Familial Amyotrophic Lateral Sclerosis", *Brain*, Vol. 139, No. 5, p. e28.

Brooks, S.P. and S.B. Dunnett, 2009, "Tests to Assess Motor Phenotype in Mice: A User's Guide", *Nature Reviews Neuroscience*, Vol. 10, No. 7, pp. 519–529.

Cappadocia, L. and C.D. Lima, 2018, "Ubiquitin-like Protein Conjugation: Structures, Chemistry, and Mechanism", *Chemical Reviews*, Vol. 118, No. 3, pp. 889–918.

Celen, A.B., 2019, "*A Novel Post-translational Modification on the Central CRISPR enzyme: Discovery of CAS9 Ubiquitylation"*, M.S. Thesis, Boğaziçi University.

Celen, A.B. and U. Sahin, 2020, "Sumoylation on Its 25th Anniversary: Mechanisms, Pathology, and Emerging Concepts", *The FEBS Journal*, Vol. 287, No. 15, pp. 3110–3140.

Chang, H.M. and E.T.H. Yeh, 2020, "SUMO: From Bench to Bedside", *Physiological Reviews*, Vol. 100, No. 4, pp. 1599–1619.

Chen, L.C., Y.L. Hsieh, G.Y.T. Tan, T.Y. Kuo, Y.C. Chou, P.H. Hsu and W.W. Hwang-Verslues, 2021, "Differential Effects of SUMO1 and SUMO2 on Circadian Protein PER2 Stability and Function", *Scientific Reports*, Vol. 11, No. 1, p. 14431.

Chen, Y., P.L. Chen, C.F. Chen, X. Jiang and D.J. Riley, 2008, "Never-in-Mitosis Related Kinase 1 Functions in DNA Damage Response and Checkpoint Control", *Cell Cycle*, Vol. 7, No. 20, pp. 3194–3201.

Dangoumau, A., C. Veyrat-Durebex, H. Blasco, J. Praline, P. Corcia, C.R. Andres and P. Vourc'h, 2013, "Protein SUMOylation, an Emerging Pathway in Amyotrophic Lateral Sclerosis", *International Journal of Neuroscience*, Vol. 123, No. 6, pp. 366–374.

Ergünay, T., Ö. Ayhan, A.B. Celen, P. Georgiadou, E. Pekbilir, Y.T. Abaci, D. Yesildag, M. Rettel, U. Sobhiafshar, A. Ogmen, N.C. Tolga Emre and U. Sahin, 2022, "Sumoylation of Cas9 at Lysine 848 Regulates Protein Stability and DNA Binding", *Life Science Alliance*, Vol. 5, No. 4, p. e202101078.

Feige, E., O. Shalom, S. Tsuriel, N. Yissachar and B. Motro, 2006, "Nek1 Shares Structural and Functional Similarities with NIMA Kinase", *Biochimica et Biophysica Acta (BBA) - Molecular Cell Research*, Vol. 1763, No. 3, pp. 272–281.

Jasin, M. and R. Rothstein, 2013, "Repair of Strand Breaks by Homologous Recombination", *Cold Spring Harbor Perspectives in Biology*, Vol. 5, No. 11, p. a012740.

Jiang, F., and J.A. Doudna, 2017, "CRISPR–Cas9 Structures and Mechanisms", *Annual Review of Biophysics*, Vol. 46, No. 1, pp. 505–529.

Josa-Prado, F., J.M. Henley and K.A. Wilkinson, 2015, "SUMOylation of Argonaute-2 Regulates RNA Interference Activity", *Biochemical and Biophysical Research Communications*, Vol. 464, No. 4, pp. 1066–1071.

Kenna, K.P., P.T.C. van Doormaal, A.M. Dekker, N. Ticozzi, B.J. Kenna, F. P. Diekstra, W. van Rheenen, K.R. van Eijk, A.R. Jones, P. Keagle, A. Shatunov, W. Sproviero, B.N. Smith, M.A. van Es, S.D. Topp, A. Kenna, J.W. Miller, C. Fallini, C. Tiloca, R.L. McLaughlin, C. Vance, C. Troakes, C. Colombrita, G. Mora, A. Calvo, F. Verde, S. Al-Sarraj, A. King, D. Calini, J. de Belleroche, F. Baas, A.J. van der Kooi, M. de Visser, A.L. Ten Asbroek, P.C. Sapp, D. McKenna-Yasek, M. Polak, S. Asress, J.L. Muñoz-Blanco, T.M. Strom, T. Meitinger, K.E. Morrison; SLAGEN Consortium, G. Lauria, K.L. Williams, P.N. Leigh, G.A. Nicholson, I.P. Blair, C.S. Leblond, P.A. Dion, G.A. Rouleau, H. Pall, P.J. Shaw, M.R. Turner, K. Talbot, F. Taroni, K.B. Boylan, M. Van Blitterswijk, R. Rademakers, J. Esteban-Pérez, A. García-Redondo, P. Van Damme, W. Robberecht, A. Chio, C. Gellera, C. Drepper, M. Sendtner, A. Ratti, J.D. Glass, J.S. Mora, N. A. Basak, O. Hardiman, A.C. Ludolph, P.M. Andersen, J.H. Weishaupt, R. H. Brown Jr, A. Al-Chalabi, V. Silani, C.E. Shaw, L.H. van den Berg, J.H. Veldink and J.E. Landers, 2016, "NEK1 Variants Confer Susceptibility to Amyotrophic Lateral Sclerosis", *Nature Genetics*, Vol. 48, No. 9, pp. 1037–1042.

Kiernan, M.C., S. Vucic, B.C. Cheah, M.R. Turner, A. Eisen, O. Hardiman, J.R. Burrell and M.C. Zoing, 2011, "Amyotrophic Lateral Sclerosis", *The Lancet*, Vol. 377, No. 9769, pp. 942–955.

Lallemand-Breitenbach, V. and H. de Thé, 2018, "PML Nuclear Bodies: From Architecture to Function", *Current Opinion in Cell Biology*, Vol. 52, pp. 154–161.

Liebelt, F. and A.C.O. Vertegaal, 2016, "Ubiquitin-Dependent and Independent Roles of SUMO in Proteostasis", *American Journal of Physiology-Cell Physiology*, Vol. 311, No. 2, pp. C284–C296.

Liu, Z., H. Dong, Y. Cui, L. Cong and D. Zhang, 2020, "Application of Different Types of CRISPR/Cas-Based Systems in Bacteria", *Microbial Cell Factories*, Vol. 19, No. 1, p. 172.

Lo, A. and L. Qi, 2017, "Genetic and Epigenetic Control of Gene Expression by CRISPR–Cas Systems", *F1000Research*, Vol. 6, p. 747.

Luo, H.B., Y.Y. Xia, X.J. Shu, Z.C. Liu, Y. Feng, X.H. Liu, G. Yu, G. Yin, Y.S. Xiong, K. Zeng, J. Jiang, K. Ye, X.C. Wang and J.Z. Wang, 2014, "SUMOylation at K340 Inhibits Tau Degradation through Deregulating Its Phosphorylation and Ubiquitination", *Proceedings of the National Academy of Sciences*, Vol. 111, No. 46, pp. 16586–16591.

Ma Y., L. Zhang, and X. Huang, 2014, "Genome Modification by CRISPR/Cas9", *The FEBS Journal*, Vol. 281, No. 23, pp. 5186–5193.

Mali, P., K.M. Esvelt and G.M. Church, 2013, "Cas9 as a Versatile Tool for Engineering Biology", *Nature Methods*, Vol. 10, No. 10, pp. 957–963.

Matic, I., M. van Hagen, J. Schimmel, B. Macek, S.C. Ogg, M.H. Tatham, R.T. Hay, A. I. Lamond, M. Mann and A.C.O. Vertegaal, 2008, "In Vivo Identification of Human Small Ubiquitin-like Modifier Polymerization Sites by High Accuracy Mass Spectrometry and an in Vitro to in Vivo Strategy", *Molecular & Cellular Proteomics*, Vol. 7, No. 1, pp. 132–144.

Mejzini, R., L.L. Flynn, I.L. Pitout, S. Fletcher, S.D. Wilton and P.A. Akkari, 2019, "ALS Genetics, Mechanisms, and Therapeutics: Where Are We Now?", *Frontiers in Neuroscience*, Vol. 13, p. 1310.

Melo-Hanchuk, T.D., P.F. Slepicka, G.V. Meirelles, F.L. Basei, D.V. Lovato, D.C. Granato, B.A. Pauletti, R.R. Domingues, A.F.P. Leme, A.L. Pelegrini, G. Lenz, S. Knapp, J.M.

Elkins and J. Kobarg, 2017, "NEK1 Kinase Domain Structure and Its Dynamic Protein Interactome after Exposure to Cisplatin", *Scientific Reports*, Vol. 7, No. 1, p. 5445.

Meluh, P.B. and D. Koshland, 1995, "Evidence That the MIF2 Gene of Saccharomyces Cerevisiae Encodes a Centromere Protein with Homology to the Mammalian Centromere Protein CENP-C", *Molecular Biology of the Cell*, Vol. 6, No. 7, pp. 793–807.

Mete, B., E. Pekbilir, B.N. Bilge, P. Georgiadou, E. Çelik, T. Sutlu, F. Tabak and U. Sahin, 2022, "Human Immunodeficiency Virus Type 1 Impairs Sumoylation", *Life Science Alliance*, Vol. 5, No. 6, p. e202101103.

Miranda, M. and A. Sorkin, 2007, "Regulation of Receptors and Transporters by Ubiquitination: New Insights into Surprisingly Similar Mechanisms", *Molecular Interventions*, Vol. 7, No. 3, p. 157–167.

Monroe, G.R., I.F. Kappen, M.F. Stokman, P.A. Terhal, M.J. H. van den Boogaard, S.M. Savelberg, L.T. van der Veken, R.J. van Es, S.M. Lens, R.C. Hengeveld, M.A. Creton, N.G. Janssen, A.B. Mink van der Molen, M.B. Ebbeling, R.H. Giles, N. v Knoers and G. van Haaften, 2016, "Compound Heterozygous NEK1 Variants in Two Siblings with Oral-Facial-Digital Syndrome Type II (Mohr Syndrome)", *European Journal of Human Genetics*, Vol. 24, No. 12, pp. 1752–1760.

Öztürk, H., 2015, "*Investigation of the Pathogenic Basis of NEK1-linked Amyotrophic Lateral Sclerosis and Discovery of a Potentian Treatment That Prevents Protein Aggregation Through Targeted Destruction"*, M.S. Thesis, Boğaziçi University.

Peng, P.H., K.W. Hsu and K.J. Wu, 2021, "Liquid-Liquid Phase Separation (LLPS) in Cellular Physiology and Tumor Biology", *American Journal of Cancer Research*, Vol. 11, No. 8, pp. 3766–3776.

Rheenen, W.V., S.L. Pulit, A.M. Dekker, A.A. Khleifat, W.J. Brands, A. Iacoangeli, K.P. Kenna, E. Kavak, M. Kooyman, R.L. McLaughlin, B. Middelkoop, M. Moisse, R.D. Schellevis, A. Shatunov, W. Sproviero, G.H.P. Tazelaar, R.A.A.V. der Spek, P.T.C.V. Doormal, K.R.V. Eijk, J.V. Vugt, A.N. Basak, I.P. Blair, J.D. Glass, O. Hardiman, W. Hide, J.E. Landers, J.S. Mora, K.E. Morrison, S. Newhouse, W. Robberecht, C.E. Shaw, P.J. Shaw, P.V. Damme, M.A.V. Es, N.R. Wray, A. Al-Chalabi, L.H.V. den Berg, and J.H. Veldink, 2018, "Project MinE: Study Design and Pilot Analyses of a Large-Scale Whole-Genome Sequencing Study in Amyotrophic Lateral Sclerosis", *European Journal of Human Genetics*, Vol. 26, No. 10, pp. 1537–1546.

Ptak, C. and R.W. Wozniak, 2017, "SUMO Regulation of Cellular Processes", *Advances in Experimental Medicine and Biology*, Vol. 963, pp. 111–126.

Ramazi, S. and J. Zahiri, 2021, "Post-Translational Modifications in Proteins: Resources, Tools and Prediction Methods", *Database*, Vol. 2021, p. baab012.

Rape, M., 2018, "Ubiquitylation at the Crossroads of Development and Disease", *Nature Reviews Molecular Cell Biology*, Vol. 19, No. 1, pp. 59–70.

Rial, D., A.A. Castro, N. Machado, P. Garção, F.Q. Gonçalves, H.B. Silva, Â.R. Tomé, A. Köfalvi, O. Corti, R. Raisman-Vozari, R.A. Cunha and R.D. Prediger, 2014, "Behavioral Phenotyping of Parkin-Deficient Mice: Looking for Early Preclinical Features of Parkinson's Disease", *PLoS ONE*, Vol. 9, No. 12, p. e114216.

Ribet, D., M. Hamon, E. Gouin, M.A. Nahori, F. Impens, H. Neyret-Kahn, K. Gevaert, J. Vandekerckhove, A. Dejean and P. Cossart, 2010, "Listeria Monocytogenes Impairs SUMOylation for Efficient Infection", *Nature*, Vol. 464, No. 7292, pp. 1192–1195.

Sahin, U., H. de Thé and V. Lallemand-Breitenbach, 2014, "PML Nuclear Bodies: Assembly and Oxidative Stress-Sensitive Sumoylation", *Nucleus*, Vol. 5, No. 6, pp. 499–507.

Shahpasandzadeh, H., B. Popova, A. Kleinknecht, P.E. Fraser, T.F. Outeiro and G.H. Braus, 2014, "Interplay between Sumoylation and Phosphorylation for Protection against α-Synuclein Inclusions", *Journal of Biological Chemistry*, Vol. 289, No. 45, pp. 31224–31240.

Siddique, N., and T. Siddique, 2021, *Amyotrophic Lateral Sclerosis Overview*, Second Edition, GeneReviews, Seattle.

Slaymaker, I.M., L.Gao, B. Zetsche, D.A. Scott, W.X. Yan and F. Zhang, 2016, "Rationally Engineered Cas9 Nucleases with Improved Specificity", *Science*, Vol. 351, No. 6268, pp. 84–88.

Sutoko, S., A. Masuda, A. Kandori, H. Sasaguri, T. Saito, T.C. Saido and T. Funane, 2021, "Early Identification of Alzheimer's Disease in Mouse Models: Application of Deep Neural Network Algorithm to Cognitive Behavioral Parameters", *IScience*, Vol. 24, No. 3, p. 102198.

Swatek, K.N. and D. Komander, 2016, "Ubiquitin Modifications", *Cell Research*, Vol. 26, No. 4, pp. 399–422.

Ulman, A., T. Levin, B. Dassa, A. Javitt, A. Kacen, M.D. Shmueli, A. Eisenberg-Lerner, D. Sheban, S. Fishllevich, E.D. Levy and Y. Merbl. 2021, "Altered Protein Abundance and Localization Inferred from Sites of Alternative Modification by Ubiquitin and SUMO", *Journal of Molecular Biology*, Vol. 433, No. 21, p. 167219.

Upadhya, P., E.H. Birkenmeier, C.S. Birkenmeier and J.E. Barker, 2000, "Mutations in a NIMA-Related Kinase Gene, Nek1, Cause Pleiotropic Effects Including a Progressive Polycystic Kidney Disease in Mice", *Proceedings of the National Academy of Sciences of the United States of America*, Vol. 97, No. 1, pp. 217–221.

Van der Spek, R.A.A., W. van Rheenen, S.L. Pulit, K.P. Kenna, L.H. van den Berg and J.H. Veldink, 2019, "The Project MinE Databrowser: Bringing Large-Scale Whole-Genome Sequencing in ALS to Researchers and the Public", *Amyotrophic Lateral Sclerosis and Frontotemporal Degeneration*, Vol. 20, No. 5–6, pp. 432–440.

Vaughan, R.M., A. Kupai and S.B. Rothbart, 2021, "Chromatin Regulation through Ubiquitin and Ubiquitin-like Histone Modifications", *Trends in Biochemical Sciences*, Vol. 46, No. 4, pp. 258–269.

Wang, H., M. la Russa and L.S. Qi, 2016, "CRISPR/Cas9 in Genome Editing and Beyond", *Annual Review of Biochemistry*, Vol. 85, No. 1, pp. 227–264.

Wang, Z., E. Horemuzova, A. Iida, L. Guo, Y. Liu, N. Matsumoto, G. Nishimura, A. Nordgren, N. Miyake, E. Tham, G. Grigelioniene and S. Ikegawa, 2017, "Axial Spondylometaphyseal Dysplasia Is Also Caused by NEK1 Mutations", *Journal of Human Genetics*, Vol. 62, No. 4, pp. 503–506.

Wilson, V.G., 2017, "Viral Interplay with the Host Sumoylation System", *Springer International Publishing*, Vol. 963, pp. 359–388.

Yao, L., X. He, B. Cui, F. Zhao and C. Zhou, 2021, "NEK1 Mutations and the Risk of Amyotrophic Lateral Sclerosis (ALS): A Meta-Analysis", *Neurological Sciences*, Vol. 42, No. 4, pp. 1277–1285.

Yau, T.Y., O. Molina and A.J. Courey, 2020, "SUMOylation in Development and Neurodegeneration", *Development*, Vol. 147, No. 6, p. dev175703.

Yun, Y. and Y. Ha, 2020, "CRISPR/Cas9-Mediated Gene Correction to Understand ALS", *International Journal of Molecular Sciences*, Vol. 21, No. 11, p. 3801.

Zhang, C., R. Quan and J. Wang, 2018, "Development and Application of CRISPR/Cas9 Technologies in Genomic Editing", *Human Molecular Genetics*, Vol. 27, No. R2, pp. R79–R88.

Zhang, F., Y. Wen and X. Guo, 2014, "CRISPR/Cas9 for Genome Editing: Progress, Implications and Challenges", *Human Molecular Genetics*, Vol. 23, No. R1, pp. R40–R46.

APPENDIX A: FOOTPRINT TESTS

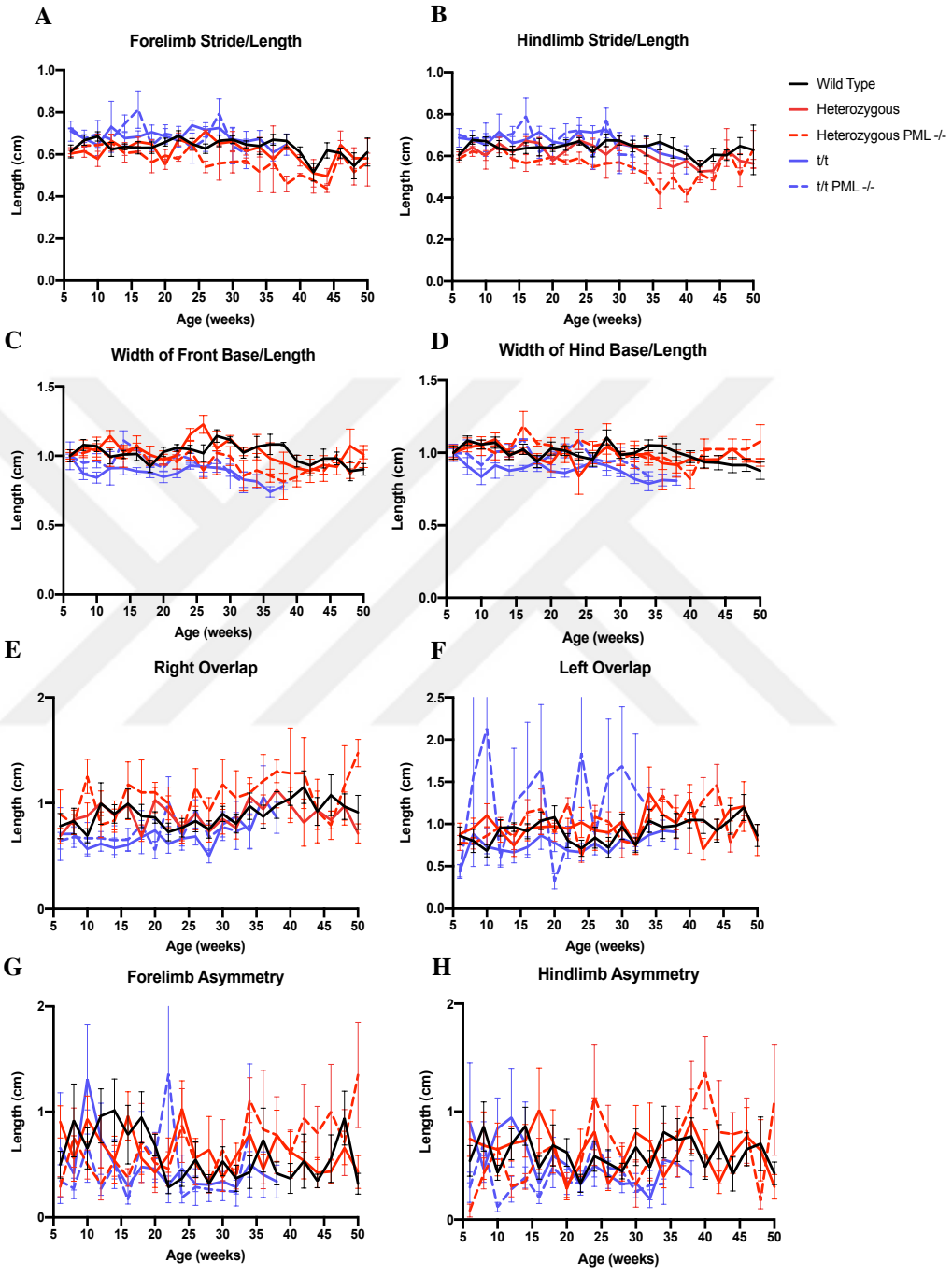

Figure A.1. Footprint test graphics. (A, B, C and D) Since stride length and base width depends on the mouse's length, results were normalized by dividing the length of mouse. (E, F, G and H) The remaining ones do not depend on the length, so no normalization was performed on those tests. There were no other significant results except the ones mentioned in chapter 5.1.7.

APPENDIX B: PERMISSONS FROM QUOTED FIGURES AND TABLES

Figure 1.1 is reprinted from Protein Phosphorylation: A Major Switch Mechanism for Metabolic Regulation, 26/12, 12, 2015, with permission from Elsevier.

Figure 1.2 is reproduced courtesy of Cell Signaling Technology, Inc.

Figure 1.4 is reprinted from Sumoylation on its 25th anniversary: mechanisms, pathology, and emerging concepts, 287/15, 31, 2020, with permission from John Wiley and Sons.

Figure 1.5 is reproduced courtesy of Taylor Francis Group, 2014, LLC.

Figure 1.7 is reprinted by permission from Springer Nature Customer Service Centre GmbH: Springer Nature European Journal of Human Genetics, Compound heterozygous NEK1 variants in two siblings with oral-facial-digital syndrome type II (Mohr syndrome), Monroe, G. R., I. F. Kappen, M. F. Stokman, P. A. Terhal, M.-J. H. van den Boogaard, S. M. Savelberg, L. T. van der Veken, R. J. van Es, S. M. Lens, R. C. Hengeveld, M. A. Creton, N. G. Janssen, A. B. Mink van der Molen, M. B. Ebbeling, R. H. Giles, N. v Knoers and G. van Haaften, 2016.

Figure 1.9 is reprinted by permission from Springer Nature Customer Service Centre GmbH: Springer Nature Methods, Cas9 as a versatile tool for engineering biology, Mali, P., K. M. Esvelt, G. M. Church, 2022.

Figure 1.10 is reprinted and reproduced from Harnessing CRISPR-Cas systems for bacterial genome editing, 23/4, 8, 2015, with permission from Elsevier.

Figure 1.11 is reprinted from Genome modification by CRISPR/Cas9, 281/23, 8, 2014, with permission from John Wiley and Sons.

(For figures from Figure 5.7 to Figure 5.15) Figures that emerged within the scope of this thesis work and whose copyrights were transferred to the publishing house were used in the thesis book by the "publishing policy valid for the reuse of the text and graphics produced by the author" on the website of the publisher. These figures are published from Life Sciences Alliance, Sumoylation of Cas9 at lysine 848 regulates protein stability and DNA binding, 5/4, 2022.